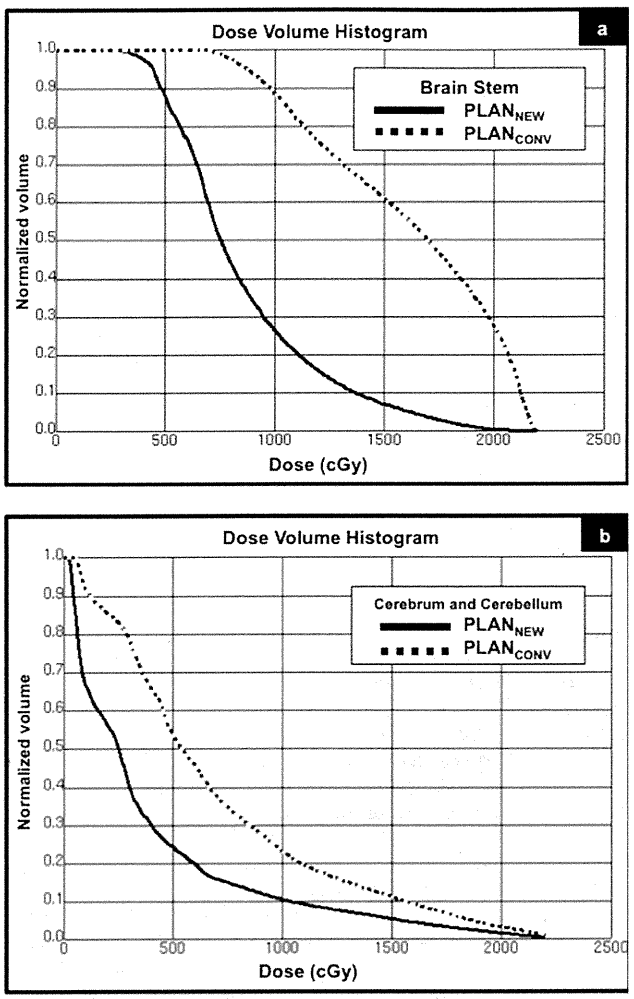

Fig. 2. DVHs of $PLAN_{NEW}$ (solid line) and $PLAN_{CONV}$ (dotted line) are as shown in Fig.1 for (a) brain stem and (b) cerebrum and cerebellum.

be an important tool for functional and molecular radiotherapy treatment planning.

References

1. Vernon MR, Maheshwari M, Schultz CJ, *et al.* Clinical outcomes of patients receiving integrated PET/CT-guided radiotherapy for head and neck carcinoma. *Int J Radiat Oncol Biol Phys* 2008;70:678–684.
2. Madani I, Duthoy W, Derie C, *et al.* Positron emission tomography-guided, focal-dose escalation using intensity-modulated radiotherapy for head and neck cancer. *Int J Radiat Oncol Biol Phys* 2007;68:126–135.
3. Guido A, Fuccio L, Rombi B, *et al.* Combined 18F-FDG-PET/CT imaging in radiotherapy target delineation for head-and-neck cancer. *Int J Radiat Oncol Biol Phys* 2009;73:759–763.
4. Ford EC, Herman J, Yorke E, *et al.* 18F-FDG PET/CT for image-guided and intensity-modulated radiotherapy. *J Nucl Med* 2009;50: 1655–1665.
5. MacManus M, Nestle U, Rosenzweig KE, *et al.* Use of PET and PET/CT for radiation therapy planning: IAEA expert report 2006–2007. *Radiother Oncol* 2009;91:85–94.
6. Ahn PH, Garg MK. Positron emission tomography/computed tomography for target delineation in head and neck cancers. *Semin Nucl Med* 2008;38:141–148.
7. Shiga T, Morimoto Y, Kubo N, *et al.* A new PET scanner with semiconductor detectors enables better identification of intratumoral inhomogeneity. *J Nucl Med* 2009;50:148–155.
8. Yanagishita N, Morimoto Y, Ishitsu T, *et al.* Physical performance of a prototype 3D PET scanner using CdTe detectors. Nuclear Science Symposium Conference Record, 2007. Vol 4. Piscataway (NJ): IEEE; 2007; 2665–2668.
9. Morimoto Y, Ueno Y, Kobashi K, *et al.* Performance of a prototype brain PET scanner based on semiconductor detectors [abstract]. *J Nucl Med* 2008;49(Suppl. 1):122P.
10. Daube-Witherspoon ME, Karp JS, Casey ME, *et al.* PET performance measurements using the NEMA NU 2–2001 standard. *J Nucl Med* 2002;43:1398–1409.
11. Adam L-E, Zaers J, Ostertag H, *et al.* Performance evaluation of the whole-body PET scanner ECAT EXACT HR+ following the IEC standard. *IEEE Trans Nucl Sci* 1997;44:1172–1179.
12. Daisne JF, Duprez T, Weynand B, *et al.* Tumor volume in pharyngolaryngeal squamous cell carcinoma: Comparison at CT, MR imaging, and FDG PET and validation with surgical specimen. *Radiology* 2004;233:93–100.
13. Heron DE, Andrade RS, Flickinger J, *et al.* Hybrid PET-CT simulation for radiation treatment planning in head-and-neck cancers: A brief technical report. *Int J Radiat Oncol Biol Phys* 2004;60: 1419–1424.
14. Riegel AC, Berson AM, Destian S, *et al.* Variability of gross tumor volume delineation in head-and-neck cancer using CT and PET/CT fusion. *Int J Radiat Oncol Biol Phys* 2006;65:726–732.
15. Nishioka T, Shiga T, Shirato H, *et al.* Image fusion between 18FDG-PET and MRI/CT for radiotherapy planning of oropharyngeal and nasopharyngeal carcinomas. *Int J Radiat Oncol Biol Phys* 2002;53: 1051–1057.
16. Ciernik IF, Dizendorf E, Baumert BG, *et al.* Radiation treatment planning with an integrated positron emission and computer tomography (PET/CT): A feasibility study. *Int J Radiat Oncol Biol Phys* 2003;57:853–863.
17. Schinagl DA, Vogel WV, Hoffmann AL, *et al.* Comparison of five segmentation tools for 18F-fluoro-deoxy-glucose-positron emission tomography-based target volume definition in head and neck cancer. *Int J Radiat Oncol Biol Phys* 2007;69:1282–1289.
18. Nestle U, Kremp S, Schaefer-Schuler A, *et al.* Comparison of different methods for delineation of 18F-FDG PET-positive tissue for target volume definition in radiotherapy of patients with non-Small cell lung cancer. *J Nucl Med* 2005;46:1342–1348.
19. Hong R, Halama J, Bova D, *et al.* Correlation of PET standard uptake value and CT window-level thresholds for target delineation in CT-based radiation treatment planning. *Int J Radiat Oncol Biol Phys* 2007;67:720–726.
20. Burri RJ, Rangaswamy B, Kostakoglu L, *et al.* Correlation of positron emission tomography standard uptake value and pathologic specimen size in cancer of the head and neck. *Int J Radiat Oncol Biol Phys* 2008;71:682–688.
21. Koshy M, Paulino AC, Howell R, *et al.* F-18 FDG PET-CT fusion in radiotherapy treatment planning for head and neck cancer. *Head Neck* 2005;27:494–502.
22. Bradley J, Thorstad WL, Mutic S, *et al.* Impact of FDG-PET on radiation therapy volume delineation in non-small-cell lung cancer. *Int J Radiat Oncol Biol Phys* 2004;59:78–86.
23. Rembielak A, Price P. The role of PET in target localization for radiotherapy treatment planning. *Onkologie* 2008;31:57–62.
24. Gregoire V, Bol A, Geets X, *et al.* Is PET-based treatment planning the new standard in modern radiotherapy? The head and neck paradigm. *Semin Radiat Oncol* 2006;16:232–238.
25. Gregoire V, Haustermans K, Geets X, *et al.* PET-based treatment planning in radiotherapy: A new standard? *J Nucl Med* 2007;48(Suppl 1): 68S–77S.
26. Troost EG, Schinagl DA, Bussink J, *et al.* Innovations in radiotherapy planning of head and neck cancers: Role of PET. *J Nucl Med*;51:66–76.

Cancer Science
The official journal of the Japanese Cancer Association JCA

Review Article

Real-time 4-D radiotherapy for lung cancer

Hiroki Shirato,[1,4] Rikiya Onimaru,[1] Masayori Ishikawa,[2] Jun-ichi Kaneko,[3] Tsuguhide Takeshima,[1] Kenta Mochizuki,[1] Shinichi Shimizu[1] and Kikuo Umegaki[1]

Departments of [1]Radiation Medicine, [2]Medical Physics, Graduate School of Medicine, [3]Quantum Science and Engineering, Graduate School of Engineering, Hokkaido University, Sapporo, Japan

(Received September 9, 2011/Accepted September 14, 2011/Accepted manuscript online September 29, 2011/Article first published online November 14, 2011)

Respiratory motion considerably influences dose distribution, and thus clinical outcomes in radiotherapy for lung cancer. Breath holding, breath coaching, respiratory gating with external surrogates, and mathematical predicting models all have inevitable uncertainty due to the unpredictable variations of internal tumor motion. The amplitude of the same tumor can vary with standard deviations >5 mm occurring in 23% of T1–2N0M0 non-small cell lung cancers. Residual motion varied 1–6 mm (95th percentile) for the 40% duty cycle of respiratory gating with external surrogates. The 4-D computed tomography is vulnerable to problems relating to the external surrogates. Real-time 4-D radiotherapy (4DRT), where the temporal changes in anatomy during the delivery of radiotherapy are explicitly considered in real time, is emerging as a new method to reduce these known sources of uncertainty. Fluoroscopic, real-time tumor-tracking technology using internal fiducial markers near the tumor has ±2 mm accuracy, and has achieved promising clinical results when used with X-ray therapy. Instantaneous irradiation based on real-time verification of internal fiducial markers is considered the minimal requisite for real-time 4DRT of lung cancers at present. Real-time tracking radiotherapy using gamma rays from positron emitters in tumors is in the preclinical research stage, but has been successful in experiments in small animals. Real-time tumor tracking via spot-scanning proton beam therapy has the capability to cure large lung cancers in motion, and is expected to be the next-generation real-time 4DRT. (*Cancer Sci* 2012; 103: 1–6)

Automatic collimation of radiation beams in real space with the aid of computer simulation in virtual space has enabled physicians to create complex dose distributions in real space and crystallized as 3-D conformal radiotherapy and intensity-modulated radiotherapy.[1] Consequently, the need for precise registration of virtual space to real space in daily treatment has become critically important. For the precise registration of static virtual space to real space, stereotactic body radiotherapy (SBRT), using a rigid external fixation device on the body, and image-guided radiotherapy, using online imaging of internal structures, have been established.[2,3] Real-time tumor-tracking radiotherapy (RTRT) was developed in 1999 to amplify the precision of irradiation of moving lung tumors.[4] We are now entering a real-time 4-D radiotherapy (4DRT) era, where the temporal changes in anatomy during the delivery of radiotherapy are explicitly considered in real time by the precise registration of dynamic virtual space to dynamic real space, for the purpose of achieving the optimal dose distribution in dynamic real space.

Stereotactic body radiotherapy

The peripheral lung parenchyma consists of many independent functional subunits. Radiation-induced pneumonitis (RP) can be avoided if we concentrate the radiation dose to the small volume, while keeping the mean lung dose (MLD) lower than its tolerance level. Using thin-slice computed tomography (CT) for planning, and a sufficient margin for the organ motion, with the aid of a body frame or imaging devices, the interfractional setup error can be 5 mm or less in SBRT of lung cancer.[5–9] Clinical studies have shown that SBRT alone can cure T1N0M0 non-small cell lung cancers, with little adverse reaction.[5–7] For 65 T1N0M0 tumors, the local control rate at 5 years was 92%, and the RP (≥grade III) rate was 1%, with a median follow-up period of 55 months.[6] The 5-year overall survival rate for Stage IA was 72%. Correcting the effect of dose per fraction, the biologically-effective dose (BED) to the tumor was 116 Gy (range: 100–141 Gy).

Considering that conventional fractionated radiotherapy (CFRT) can deliver a BED of only 72–80 Gy (60–66 Gy using 2 Gy/fraction) to the tumor, SBRT has been successful at delivering a much higher tumor dose, by taking advantage of the structure of the peripheral lung parenchyma. However, tumors having large organ motion, large volume, or are located near the trachea, main bronchus, and main vascular trunk, are not suitable for high-dose SBRT.[10,11] The risk of RP has recently been shown to increase with MLD, with a normalized total dose corrected using α/β ratio of 3 Gy[12]. The relationship of RP with single nucleotide polymorphisms is also suggested.[13]

Internal motion of lung cancer

In accordance with the clinical success of SBRT for lung cancers, the control of respiratory motion is emerging as important for reducing the unnecessary irradiation of normal tissue. Treatment planning of lung cancer using CT images is subject to individual differences in respiratory motion.[14] The concept of 4DRT, where the temporal changes in anatomy are explicitly considered during the imaging, planning, and delivery of radiotherapy, was introduced in 2000.[15] Since then, fiducial gold markers have emerged as the most reliable means of tracking the motion of lung cancer in real time during radiotherapy.[16,17] The concept of 4DRT has been improved further and integrated into other systems.[18–20]

Since 3-D coordinates of the gold markers are recorded every 0.033 s using an RTRT system, the marker motion can be regarded as a surrogate of tumor motion, as long as the marker does not migrate. In general, the amplitude of the lung tumor motion is the largest in the craniocaudal direction, followed by the anteroposterior direction, and finally the right–left direction, and it is larger in the lower and outer lung fields, although this pattern can change considerably in diseased lungs.[21,22] The average amplitudes were larger than 10 mm in approximately 33% of lung cancers.[23] The amplitude and speed can vary

[4]To whom correspondence should be addressed.
E-mail: shirato@med.hokudai.ac.jp

doi: 10.1111/j.1349-7006.2011.02114.x

considerably among treatment days for the same patient; the SD of the absolute amplitude was larger than 5 mm in 23% of lung cancer cases. Tumor position in the exhalation phase was shown to be more stable than that in the inhalation phase, so that tumor position upon exhalation was suggested to be more appropriate as the baseline for gated radiotherapy. However, the tumor position, even at the exhale phase, often shifts more than 2 mm during treatment. On average, four readjustments of the table position were necessary during each treatment session (30–40 min) due to baseline shifts of the tumor position of more than 2 mm.[23] Furthermore, there is a ''hysteresis''; the trajectory of the marker during inhalation is often different than that at exhalation, so we need to monitor the hysteresis in gating and scanning of the beam for moving tumors.[16] Therefore, among the treatment techniques in which a narrow therapeutic beam is moved or scanned along the predicted trajectory of the tumor, there can be serious discrepancy between the planning and motion of the beam. The probability density of the trajectory of the marker detected before radiotherapy is expected to be useful for treatment planning of real-time 4DRT (Fig. 1). A dynamic internal margin based on the probability density is expected to improve the efficiency of beam usage.[24]

External surrogates

Instead of implantation of internal fiducial markers, external surrogates are expected to be useful for respiratory gating. The combination of external surrogates and internal observation with simple prediction models was suggested to reduce the residual motion of the tumor in a simulation study.[25] However, a lack of correlation between external signals and internal tumor positions during breathing and breath-hold periods have been reported.[26–28] The residual motion varied between 0.9 and 6.2 mm (95th percentile) for 40% duty-cycle windows, and large fluctuations (>300%) were seen in the residual motion between some beams in respiration gating with an external surrogate.[29] When tumor position was predicted based on the external surrogates, the baseline shift of tumor position was the major source of targeting error.[30] The absolute change in mean tumor position from the first 10-min block to the third 10-min block was >5 mm in 13% of 55 treatment fractions in lung cancer treatment.[31]

4-D CT (4DCT) with a respiration-gating system using external surrogates has been reported to be effective in reducing uncertainty in treatment planning for lung tumors.[32] However, the 4DCT images are all vulnerable to problems relating to the lack of correlation between external surrogates and internal tumor positions during breathing.

Breath coaching and holding

Audiovisual biofeedback is often used to help individuals maintain a regular breathing rhythm or to hold their breath during treatment.[33–35] However, the effectiveness of visual coaching for tumor localization is still debatable, given variations in observers, lengths of observation times, and different research methods.[28,36–38] Neicu *et al.*[37] pointed out that biofeedback is not useful coaching for patients with medical or respiratory difficulty, while in fact, those patients actually need to be coached more than anyone else. The registration between virtual dynamic space in CT plan and real dynamic space in actual treatment has uncertainty, because CT is studied in a limited time period (<5 min) compared to the treatment delivery (10–40 min). Differences in tumor positions exceeding 5 mm between coached and uncoached 4DCT scans were detected in up to 56% of mobile tumors.[39] It is still uncertain whether breath coaching is reliable enough to reduce the internal residual motion of the tumor during the beam-on period.

Prediction of organ motion

The prediction of internal motion is expected to be useful for 4DRT to reduce intrafractional error, but it is not so simple. The instantaneous maximum speed of lung cancer can be more than

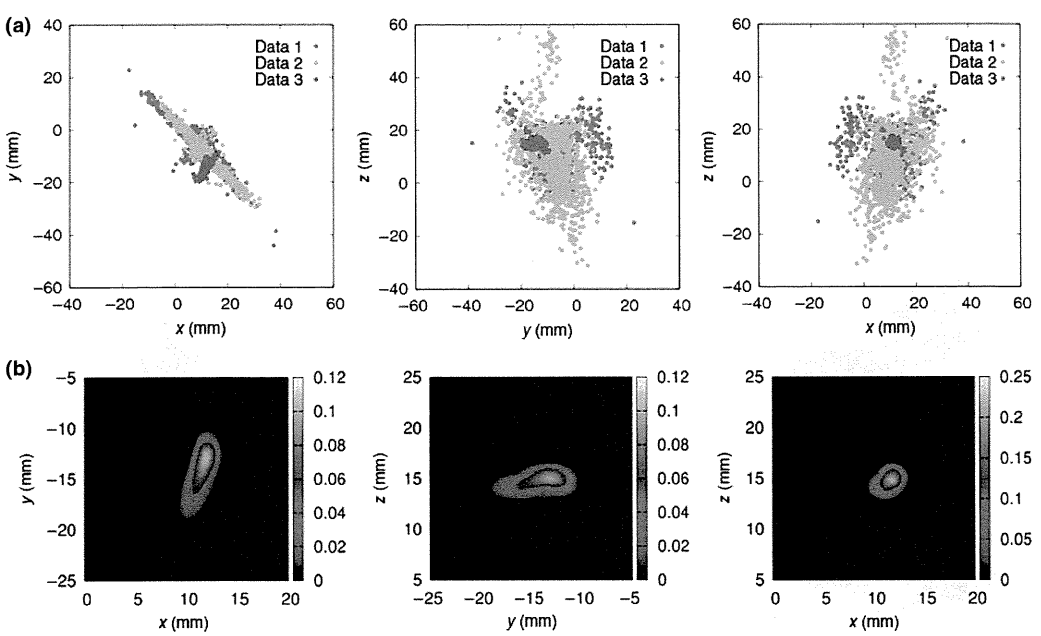

Fig. 1. Variation of trajectory and density distribution of tumor position. (a) Plots of three data sets (data 1–3) of the trajectory of the same fiducial marker along the *xy*, *yz*, and *zx* coordinates in the same treatment session showed a variety of trajectories. (b) Probability density distribution of the trajectory of the same fiducial marker made from data 1. It shows that the probability density of data 1 was in fact similar to the trajectory map of data 3.

doi: 10.1111/j.1349-7006.2011.02114.x

33 mm/s in 29% of patients, and variable in the same patient.[23] The latency period can be <100 ms in electronic gating, but might be longer in mechanical tracking systems, such as robotics and multileaf collimators.[40,41] The respiratory patterns are not simple sine curves, and can be categorized into several types: regular breathing, frequency changes, baseline shifts, amplitude changes, cardiac motion, or combination patterns.[42] In terms of overall error in predicting respiratory motion, the adaptive filter model-based prediction algorithm performs better than the sinusoidal model.[43] Linear filtering, Kalman filtering, neural networks, local regression, autoregressive-moving average model, and others have been reported to reduce error in prediction.[44–48] These models are usable for a regular breathing pattern, but are not yet clinically reliable enough for other respiratory patterns.

Real-time tumor-tracking radiotherapy

Real-time tumor-tracking radiotherapy consists of two parts: (i) real-time monitoring of tumor position using tracking technology in computer science; and (ii) instantaneous irradiation technology. There have been two instantaneous irradiation methods: (i) pursuing irradiation, where the therapeutic beam changes its direction during treatment; and (ii) interrupting irradiation, where the therapeutic beam does not change its direction.[40] By definition, pursuing irradiation without real-time monitoring, but with some prediction models, is not included in RTRT. The prototype RTRT system used the interrupting irradiation method. The system recognizes the 3-D coordinates of a gold marker (1.5 mm) in or around the tumor 30 times/s using the two fluoroscopic X-ray systems. The linear accelerator is gated to irradiate the tumor only when the marker is within ±1–2 mm from its planned coordinates relative to the isocenter. The geometric accuracy of the system is not deteriorated by the unpredictable respiratory motion up to a speed of 40 mm/s. Debates regarding the uncertainty of the migration of markers have been clarified by the clinical studies of RTRT with strict quality control, which showed excellent results for lung cancers, liver cancers, and others.[49–51] Real-time tumor monitoring without fiducial markers for peripheral radiodense tumors is appealing, but is still unreliable for the majority of patients.[52] At present, instantaneous irradiation based on real-time verification of internal fiducial markers is appreciated as the minimal requisite for real-time 4DRT of lung cancers.

Molecular tracking radiotherapy

Positron emission tomography can improve the precision of determinations of the extent of lung cancer, and positron emission markers have been proposed as fiducial markers, instead of metallic markers, in RTRT.[53–56] Positron-sensitive detectors are used to record coincident annihilation gamma rays from fiducial positron emission markers implanted in or around the tumor. Cancers in small animals have been cured using a positron emitter as the surrogate of tumor motion (Fig. 2).[54] A parallel-plane PET system has been developed to be attached to a linear accelerator for molecular-base patient setup verification.[57] If we can detect the real-time distribution of hypoxic cells during radiotherapy using the parallel-plane PET system, a real-time boost of the dose to the radio-resistant cancer cells will be realized, even when temporal change in the hypoxic region in the tumor is apparent.[58,59]

Real-time tumor-tracking, spot-scanning proton beam therapy

Proton beam therapy (PBT) has physical advantages over X-ray therapy, especially for large cancers, because of the Bragg peak.[60–63] The clinical outcome of lung cancers is expected to be improved with PBT.[64–68] Although debates exist about the requirement of randomized, clinical trials to confirm the benefit of expensive PBT systems, PBT technology is improving rapidly, and hospital-based PBT systems are now increasing in number (Fig. 3).[66–68] Active spot-scanning PBT is known as a new-generation PBT, whose advantages include a large field size (maximum 30 × 40 cm), little contamination by neutrons (lower carcinogenesis), flexibility in the number of beams (better dose distribution), and the capability for intensity-modulated PBT.[69–72] The size of the machine and building can be reduced, and the total cost-effectiveness improved if the PBT machine is dedicated to active spot scanning.

Large cancers in moving organs, such as T3N1M0 non-small cell lung cancers and large hepatocellular carcinomas, are problems than can be overcome by the new-generation PBT.[73] Real-time tumor-tracking, spot-scanning PBT, that is, real-time 4-D PBT, might be a solution.

Carbon beam therapy, which has a Bragg peak as a proton beam and sharper lateral dose distribution than a proton beam, achieved an excellent local control rate for rare malignant tumors resistant to CFRT.[74] However, the advantage of carbon beam therapy compared to PBT has yet to be determined for many cancers. Its distinct characteristics of a sharp lateral penumbra might be more useful for spot-scanning technology.[75]

The risk of second malignancies after radiotherapy strongly depends on the organ, age of the patient, dose, and the characteristics of the beam.[76] Novel risk-visualization methods are needed to facilitate routine risk-adapted, personalized clinical decision-making.

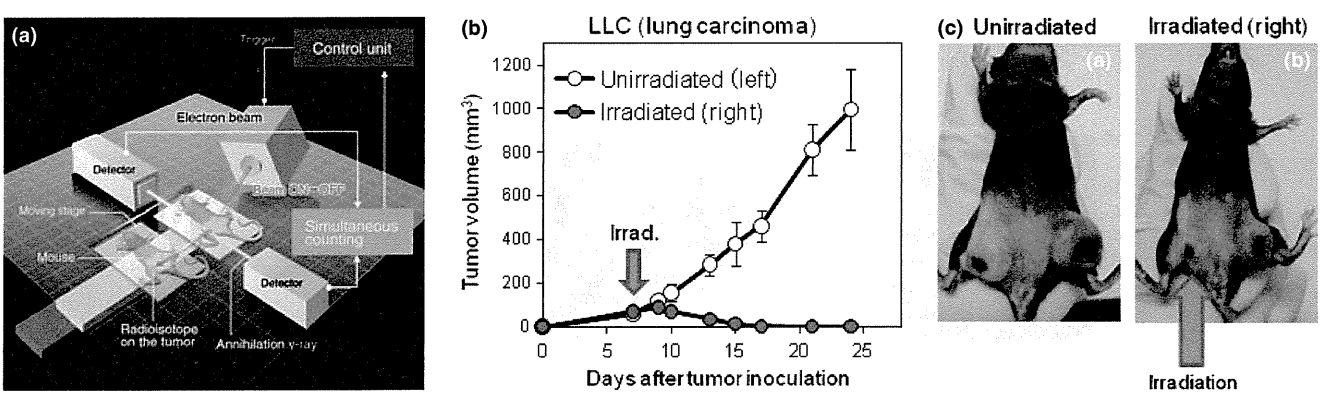

Fig. 2. Molecular tracking radiotherapy: (a) Tumor in a mouse in a moving state, which moves 15 mm/s, with an amplitude of 2 cm, was irradiated by 1.5-cm electron beam only when a radioisotope (^{22}Na source) near the tumor came into the gating window. Two sets of positron emission detectors were used. Seven days after tumor inoculation, the tumor at the right thigh was given 20 Gy. (b,c) Nine days after tumor inoculation, the irradiated tumor at the right thigh was controlled, but the unirradiated tumor at the left thigh had enlarged rapidly.

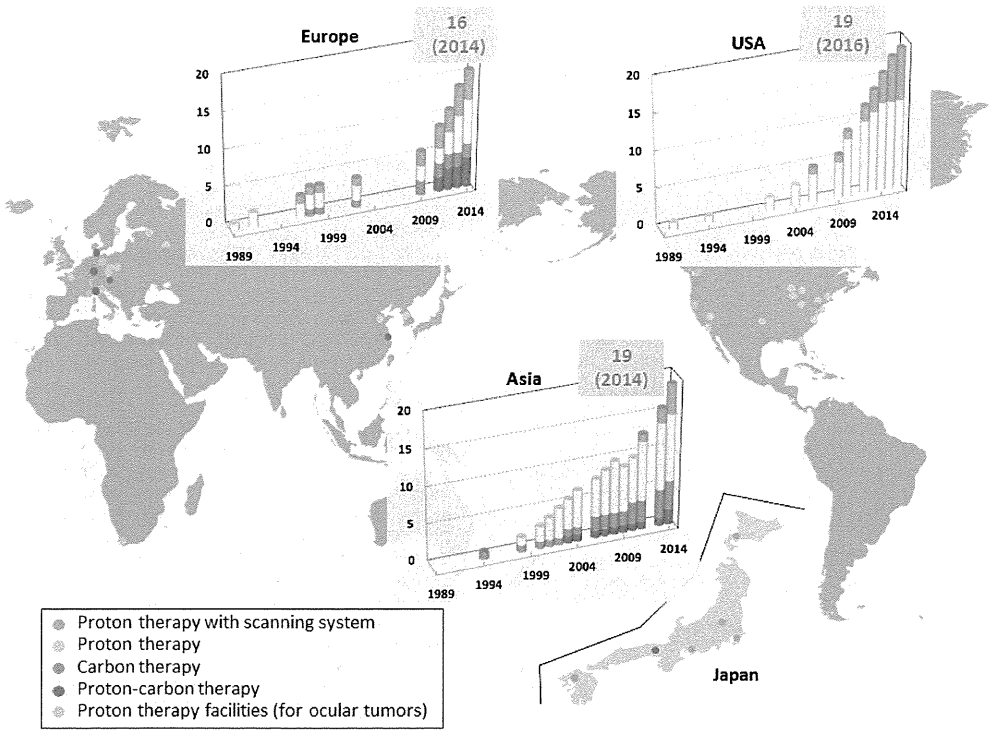

Fig. 3. Distribution of proton beam therapy centers in the world, and the number of centers, excluding those only for ocular melanoma treatment, in the USA, Europe, and Asia.

Conclusions and future remarks

The control of organ motion is emerging as a crucial objective in reducing unnecessary irradiation to normal tissue. External surrogates, breath coaching, and prediction models all require attention because of their lack of reliability in accurately localizing internal lung cancer lesions. Instantaneous irradiation based on real-time verification of internal fiducial markers is appreciated as the minimal requisite for real-time 4DRT of lung cancers at present. Molecular imaging for tumor tracking is a key area for investigation in the next decade. Real-time tumor-tracking, spot-scanning PBT is expected to open the door to the next stage of curing large tumors in moving organs.

Acknowledgment

This review is partly based on the research grant by the Japan Society for the Promotion of Science (JSPS) through the "Funding Program for World-Leading Innovative R&D on Science and Technology (FIRST Program)," initiated by the Council for Science and Technology Policy (CSTP).

Disclosure Statement

Hiroki Shirato has received research funding from Hitachi Co. Ltd. and Mitsubishi Heavy Industries Co. Ltd.

References

1 Das IJ, Cheng CW, Chopra KL, Mitra RK, Srivastava SP, Glatstein E. Intensity-modulated radiation therapy dose prescription, recording, and delivery: patterns of variability among institutions and treatment planning systems. *J Natl Cancer Inst* 2008; **100**: 300–7.

2 Verellen D, De Ridder M, Linthout N, Tournel K, Soete G, Storme G. Innovations in image-guided radiotherapy. *Nat Rev Cancer* 2007; **7**: 949–60.

3 Fowler JF, Tomé WA, Fenwick JD, Mehta MP. A challenge to traditional radiation oncology. *Int J Radiat Oncol Biol Phys* 2004; **60**: 1241–56.

4 Shirato H, Shimizu S, Shimizu T, Nishioka T, Miyasaka K. Real-time tumour-tracking radiotherapy. *Lancet* 1999; **353**: 1331–2.

5 Uematsu M, Shioda A, Suda A *et al.* Computed tomography-guided frameless stereotactic radiotherapy for stage I non-small cell lung cancer: a 5-year experience. *Int J Radiat Oncol Biol Phys* 2001; **51**: 666–70.

6 Onishi H, Shirato H, Nagata Y *et al.* Stereotactic body radiotherapy (SBRT) for operable stage i non-small-cell lung cancer: can SBRT Be comparable to surgery? *Int J Radiat Oncol Biol Phys* 2010; doi:10.1016/j.ijrobp.2009.07.1751 [Epub ahead of print].

7 Timmerman R, Paulus R, Galvin J *et al.* Stereotactic body radiation therapy for inoperable early stage lung cancer. *JAMA* 2010; **303**: 1070–6.

8 Bengua G, Ishikawa M, Sutherland K *et al.* Evaluation of the effectiveness of the stereotactic body frame in reducing respiratory intrafractional organ motion using the real-time tumor-tracking radiotherapy system. *Int J Radiat Oncol Biol Phys* 2010; **77**: 630–6.

9 Starkschall G, Balter P, Britton K, McAleer MF, Cox JD, Mohan R. Interfractional reproducibility of lung tumor location using various methods of respiratory motion mitigation. *Int J Radiat Oncol Biol Phys* 2011; **79**: 596–601.

10 Nagata Y, Hiraoka M, Mizowaki T *et al.* Survey of stereotactic body radiation therapy in Japan by the Japan 3-D Conformal External Beam Radiotherapy Group. *Int J Radiat Oncol Biol Phys* 2009; **75**: 343–7.

11 Timmerman R, McGarry R, Yiannoutsos C *et al.* Excessive toxicity when treating central tumors in a phase II study of stereotactic body radiation therapy for medically inoperable early-stage lung cancer. *J Clin Oncol* 2006; **24**: 4833–9.

12 Borst GR, Ishikawa M, Nijkamp J *et al.* Radiation pneumonitis in patients treated for malignant pulmonary lesions with hypofractionated radiation therapy. *Radiother Oncol* 2009; **91**: 307–13.

13 Yuan X, Liao Z, Liu Z *et al.* Single nucleotide polymorphism at rs1982073:T869C of the TGFbeta 1 gene is associated with the risk of radiation pneumonitis in patients with non-small-cell lung cancer treated with definitive radiotherapy. *J Clin Oncol* 2009; **27**: 3370–8.

14 Shimizu S, Shirato H, Kagei K *et al.* Impact of respiratory movement on the computed tomographic images of small lung tumors in three-dimensional (3D) radiotherapy. *Int J Radiat Oncol Biol Phys* 2000; **46**: 1127–33.

doi: 10.1111/j.1349-7006.2011.02114.x

15 Shirato H, Shimizu S, Kitamura K *et al.* Four-dimensional treatment planning and fluoroscopic real-time tumor tracking radiotherapy for moving tumor. *Int J Radiat Oncol Biol Phys* 2000; **48**: 435–42.
16 Seppenwoolde Y, Shirato H, Kitamura K *et al.* Precise and real-time measurement of 3D tumor motion in lung due to breathing and heartbeat, measured during radiotherapy. *Int J Radiat Oncol Biol Phys* 2002; **53**: 822–34.
17 Shirato H, Seppenwoolde Y, Kitamura K, Onimura R, Shimizu S. Intrafractional tumor motion: lung and liver. *Semin Radiat Oncol* 2004; **14**: 10–8.
18 Kamino Y, Takayama K, Kokubo M *et al.* Development of a four-dimensional image-guided radiotherapy system with a gimbaled X-ray head. *Int J Radiat Oncol Biol Phys* 2006; **66**: 271–8.
19 Miyamoto N, Ishikawa M, Bengua G *et al.* Optimization of fluoroscopy parameters using pattern matching prediction in the real-time tumor-tracking radiotherapy system. *Phys Med Biol* 2011; **56**: 4803–13.
20 Siddique S, Fiume E, Jaffray DA. Minimizing dose during fluoroscopic tracking through geometric performance feedback. *Med Phys* 2011; **38**: 2494–507.
21 Onimaru R, Shirato H, Fujino M *et al.* The effect of tumor location and respiratory function on tumor movement estimated by real-time tracking radiotherapy (RTRT) system. *Int J Radiat Oncol Biol Phys* 2005; **63**: 164–9.
22 Onodera Y, Nishioka N, Yasuda K *et al.* Relationship between diseased lung tissues on computed tomography and motion of fiducial marker near lung cancer. *Int J Radiat Oncol Biol Phys* 2011; **79**: 1408–13.
23 Shirato H, Suzuki K, Sharp GC *et al.* Speed and amplitude of lung tumor motion precisely detected in four-dimensional setup and in real-time tumor-tracking radiotherapy. *Int J Radiat Oncol Biol Phys* 2006; **64**: 1229–36.
24 Coolens C, Webb S, Shirato H, Nishioka K, Evans PM. A margin model to account for respiration-induced tumor motion and its variability. *Phys Med Biol* 2008; **53**: 4317–30.
25 Seppenwoolde Y, Berbeco RI, Nishioka S, Shirato H, Heijmen B. Accuracy of tumor motion compensation algorithm from a robotic respiratory tracking system: a simulation study. *Med Phys* 2007; **34**: 2774–84.
26 Ionascu D, Jiang SB, Nishioka S, Shirato H, Berbeco RI. Internal–external correlation investigations of respiratory induced motion of lung tumors. *Med Phys* 2007; **34**: 3893–903.
27 Hoisak JD, Sixel KE, Tirona R, Cheung PC, Pignol JP. Correlation of lung tumor motion with external surrogate indicators of respiration. *Int J Radiat Oncol Biol Phys* 2004; **60**: 1298–306.
28 Hunjan S, Starkschall G, Prado K, Dong L, Balter P. Lack of correlation between external fiducial positions and internal tumor positions during breath-hold CT. *Int J Radiat Oncol Biol Phys* 2010; **76**: 1586–91.
29 Berbeco RI, Nishioka S, Shirato H, Chen GT, Jiang SB. Residual motion of lung tumours in gated radiotherapy with external respiratory surrogates. *Phys Med Biol* 2005; **50**: 3655–67.
30 Zhao B, Yang Y, Li T, Li X, Heron DE, Huq MS. Statistical analysis of target motion in gated lung stereotactic body radiation therapy. *Phys Med Biol* 2011; **56**: 1385–95.
31 Malinowski K, McAvoy TJ, George R, Dietrich S, D'Souza WD. Incidence of changes in respiration-induced tumor motion and its relationship with respiratory surrogates during individual treatment fractions. *Int J Radiat Oncol Biol Phys* 2011; doi:10.1016/j.ijrobp.2011.02.048 [Epub ahead of print].
32 Vedam SS, Keall PJ, Kini VR, Mostafavi H, Shukla HP, Mohan R. Acquiring a four-dimensional computed tomography dataset using an external respiratory signal. *Phys Med Biol* 2003; **48**: 45–62.
33 Keall PJ, Mageras GS, Balter JM *et al.* The management of respiratory motion in radiation oncology report of AAPM Task Group 76. *Med Phys* 2006; **33**: 3874–900.
34 George R, Chung TD, Vedam SS *et al.* Audio-visual biofeedback for respiratory-gated radiotherapy: impact of audio instruction and audio-visual biofeedback on respiratory-gated radiotherapy. *Int J Radiat Oncol Biol Phys* 2006; **65**: 924–33.
35 Jiang SB, Wolfgang J, Mageras GS. Quality assurance challenges for motion-adaptive radiation therapy: gating, breath holding, and four-dimensional computed tomography. *Int J Radiat Oncol Biol Phys* 2008; **71**(1 Suppl): S103–7.
36 Cui G, Gopalan S, Yamamoto T, Berger J, Maxim PG, Keall PJ. Commissioning and quality assurance for a respiratory training system based on audiovisual biofeedback. *J Appl Clin Med Phys* 2010; **11**: 3262.
37 Neicu T, Berbeco R, Wolfgang J, Jiang SB. Synchronized moving aperture radiation therapy (SMART): improvement of breathing pattern reproducibility using respiratory coaching. *Phys Med Biol* 2006; **51**: 617–36.
38 Onishi H, Kawakami H, Marino K *et al.* A simple respiratory indicator for irradiation during voluntary breath holding: a one-touch device without electronic materials. *Radiology* 2010; **255**: 917–23.
39 Haasbeek CJ, Spoelstra FO, Lagerwaard FJ *et al.* Impact of audio-coaching on the position of lung tumors. *Int J Radiat Oncol Biol Phys* 2008; **71**: 1118–23.
40 Shirato H, Shimizu S, Kitamura K, Onimaru R. Organ motion in image-guided radiotherapy: lessons from real-time tumor-tracking radiotherapy. *Int J Clin Oncol* 2007; **12**: 8–16.
41 Fledelius W, Keall PJ, Cho B *et al.* Tracking latency in image-based dynamic MLC tracking with direct image access. *Acta Oncol* 2011; **50**: 952–9.
42 Wu H, Sharp GC, Salzberg B, Kaeli D, Shirato H, Jiang SB. A finite state model for respiratory motion analysis in image guided radiation therapy. *Phys Med Biol* 2004; **49**: 5357–72.
43 Vedam SS, Keall PJ, Docef A, Todor DA, Kini VR, Mohan R. Predicting respiratory motion for four-dimensional radiotherapy. *Med Phys* 2004; **31**: 2274–83.
44 Sharp GC, Jiang SB, Shimizu S, Shirato H. Prediction of respiratory tumour motion for real-time image-guided radiotherapy. *Phys Med Biol* 2004; **49**: 425–40.
45 Murphy MJ, Pokhrel D. Optimization of an adaptive neural network to predict breathing. *Med Phys* 2009; **36**: 40–7.
46 Ruan D, Fessler JA, Balter JM. Real-time prediction of respiratory motion based on local regression methods. *Phys Med Biol* 2007; **52**: 7137–52.
47 Ren Q, Nishioka S, Shirato H, Berbeco RI. Adaptive prediction of respiratory motion for motion compensation radiotherapy. *Phys Med Biol* 2007; **52**: 6651–61.
48 Roland T, Mavroidis P, Shi C, Papanikolaou N. Incorporating system latency associated with real-time target tracking radiotherapy in the dose prediction step. *Phys Med Biol* 2010; **55**: 2651–68.
49 Onimaru R, Fujino M, Yamazaki K *et al.* Steep dose-response relationship for stage I non-small-cell lung cancer using hypofractionated high-dose irradiation by real-time tumor-tracking radiotherapy. *Int J Radiat Oncol Biol Phys* 2008; **70**: 374–81.
50 Taguchi H, Sakuhara Y, Hige S *et al.* Intercepting radiotherapy using a real-time tumor-tracking radiotherapy system for highly selected patients with hepatocellular carcinoma unresectable with other modalities. *Int J Radiat Oncol Biol Phys* 2007; **69**: 376–80.
51 Sakakibara-Konishi J, Oizumi S, Kinoshita I *et al.* Phase I study of concurrent real-time tumor-tracking thoracic radiation therapy with paclitaxel and carboplatin in locally advanced non-small cell lung cancer. *Lung Cancer* 2011; **74**: 248–52.
52 Dieterich S, Gibbs IC. The CyberKnife in clinical use: current roles, future expectations. *Front Radiat Ther Oncol* 2011; **43**: 181–94.
53 Grills IS, Yan D, Black QC, Wong CY, Martinez AA, Kestin LL. Clinical implications of defining the gross tumor volume with combination of CT and 18FDG-positron emission tomography in non-small-cell lung cancer. *Int J Radiat Oncol Biol Phys* 2007; **67**: 709–19.
54 Kaneko J, Fujita F, Shirato H, Takada E. Dynamic tumor radiation treatment apparatus and dynamic tumor radiation treatment program. PCT/JP2008/052944, US 2010/0142677 A1.
55 Xu T, Wong JT, Shikhaliev PM, Ducote JL, Al-Ghazi MS, Molloi S. Real-time tumor tracking using implanted positron emission markers: concept and simulation study. *Med Phys* 2006; **33**: 2598–609.
56 Chamberland M, Wassenaar R, Spencer B, Xu T. Performance evaluation of real-time motion tracking using positron emission fiducial markers. *Med Phys* 2011; **38**: 810–9.
57 Yamaguchi S, Ishikawa M, Bengua G *et al.* A feasibility study of a molecular-based patient setup verification method using a parallel-plane PET system. *Phys Med Biol* 2011; **56**: 965–77.
58 Bentzen SM, Gregoire V. Molecular imaging-based dose painting: a novel paradigm for radiation therapy prescription. *Semin Radiat Oncol* 2011; **21**: 101–10.
59 Lin Z, Mechalakos J, Nehmeh S *et al.* The influence of changes in tumor hypoxia on dose-painting treatment plans based on 18F-FMISO positron emission tomography. *Int J Radiat Oncol Biol Phys* 2008; **70**: 1219–28.
60 Durante M, Loeffler JS. Charged particles in radiation oncology. *Nat Rev Clin Oncol* 2010; **7**: 37–43.
61 Kooy HM, Clasie BM, Lu HM *et al.* A case study in proton pencil-beam scanning delivery. *Int J Radiat Oncol Biol Phys* 2010; **76**: 624–30.
62 Sugahara S, Oshiro Y, Nakayama H *et al.* Proton beam therapy for large hepatocellular carcinoma. *Int J Radiat Oncol Biol Phys* 2010; **76**: 460–6.
63 Kooy H, Loeffler JS, DeLaney TF. Proton beam therapy. *Br J Cancer* 2005; **93**: 849–54.
64 Kadoya N, Obata Y, Kato T *et al.* Dose-volume comparison of proton radiotherapy and stereotactic body radiotherapy for non-small-cell lung cancer. *Int J Radiat Oncol Biol Phys* 2011; **79**: 1225–31.
65 Macdonald OK, Kruse JJ, Miller JM *et al.* Proton beam radiotherapy versus three-dimensional conformal stereotactic body radiotherapy in primary peripheral, early-stage non-small-cell lung carcinoma: a comparative dosimetric analysis. *Int J Radiat Oncol Biol Phys* 2009; **75**: 950–8.
66 Loeffler JS. Technology assessment in radiation oncology: time for reassessment? *Nat Clin Pract Oncol* 2008; **5**: 299.
67 Suit H, Kooy H, Trofimov A *et al.* Should positive phase III clinical trial data be required before proton beam therapy is more widely adopted? No. *Radiother Oncol* 2008; **86**: 148–53.
68 Brada M, Pijls-Johannesma M, De Ruysscher D. Current clinical evidence for proton therapy. *Cancer J* 2009; **15**: 319–24.

69 Hall EJ. Intensity-modulated radiation therapy, protons, and the risk of second cancers. *Int J Radiat Oncol Biol Phys* 2006; **65**: 1–7.
70 Smith A, Gillin M, Bues M *et al.* The M. D. Anderson proton therapy system. *Med Phys* 2009; **36**: 4068–83.
71 Gillin MT, Sahoo N, Bues M *et al.* Commissioning of the discrete spot scanning proton beam delivery system at the University of Texas M.D. Anderson Cancer Center, Proton Therapy Center, Houston. *Med Phys* 2010; **37**: 154–63.
72 af Rosenschöld PM, Aznar MC, Nygaard DE *et al.* A treatment planning study of the potential of geometrical tracking for intensity modulated proton therapy of lung cancer. *Acta Oncol* 2010; **49**: 1141–8.
73 Petersen JB, Lassen Y, Hansen AT, Muren LP, Grau C, Høyer M. Normal liver tissue sparing by intensity-modulated proton stereotactic body radiotherapy for solitary liver tumours. *Acta Oncol* 2011; **50**: 823–8.
74 Imai R, Kamada T, Tsuji H *et al.* Effect of carbon ion radiotherapy for sacral chordoma: results of phase i–ii and phase ii clinical trials. *Int J Radiat Oncol Biol Phys* 2010; **77**: 1470–6.
75 Furukawa T, Inaniwa T, Sato S *et al.* Performance of the NIRS fast scanning system for heavy-ion radiotherapy. *Med Phys* 2010; **37**: 5672–82.
76 Newhauser WD, Durante M. Assessing the risk of second malignancies after modern radiotherapy. *Nat Rev Cancer* 2011; **11**: 438–48.

doi: 10.1111/j.1349-7006.2011.02114.x

Int. J. Radiation Oncology Biol. Phys., Vol. 81, No. 4, pp. e393–e399, 2011

0360-3016/$ - see front matter

ELSEVIER

doi:10.1016/j.ijrobp.2011.04.043

CLINICAL INVESTIGATION **Prostate**

USE OF IMPLANTED MARKERS AND INTERPORTAL ADJUSTMENT WITH REAL-TIME TRACKING RADIOTHERAPY SYSTEM TO REDUCE INTRAFRACTION PROSTATE MOTION

SHINICHI SHIMIZU, M.D.,* YASUHIRO OSAKA, M.D.,* NOBUO SHINOHARA, M.D.,† ATARU SAZAWA, M.D.,† KENTARO NISHIOKA, M.D.,* RYUSUKE SUZUKI, PH.D.,‡ RIKIYA ONIMARU, M.D.,* AND HIROKI SHIRATO, M.D.*

Departments of *Radiation Medicine, †Urology, and ‡Medical Physics, Hokkaido University School of Medicine, Sapporo, Japan

Purpose: Interportal adjustment was applied to patients with prostate cancer using three fiducial markers and two sets of fluoroscopy in a real-time tumor-tracking radiotherapy (RTRT) system. The incidence of table position adjustment required to keep intrafractional uncertainty within 2.0 mm was investigated in this study.

Methods and Materials: The coordinates of the center of gravity of the three fiducial markers were measured at the start of every portal irradiation in intensity-modulated radiotherapy (IMRT) with seven ports. The table position was adjusted to the planned position if the discrepancy was larger than 2.0 mm in the anterior–posterior (AP), cranial–caudal (CC), or left–right (LR) directions. In total, we analyzed 4,541 observations in 20 patients who received 70 Gy in 30 fractions (7.6 times a day on average).

Results: The incidence of table position adjustment at 10 minutes from the initial setup of each treatment was 14.2%, 12.3%, and 5.0% of the observations in the AP, CC, and LR directions, respectively. The accumulated incidence of the table position adjustment was significantly higher at 10 minutes than at 2 minutes for AP ($p = 0.0033$) and CC ($p = 0.0110$) but not LR ($p = 0.4296$). An adjustment greater than 5 mm was required at least once in the treatment period in 11 (55%) patients.

Conclusions: Interportal adjustment of table position was required in more than 10% of portal irradiations during the 10-minute period after initial setup to maintain treatment accuracy within 2.0 mm. © 2011 Elsevier Inc.

Radiotherapy, Prostate, Intrafraction organ motion, Image-guided radiotherapy.

INTRODUCTION

Personalized radiotherapy is required in the era of personalized medicine. Organ motion can be an important patient-specific prognostic factor to improve the therapeutic ratio of radiotherapy. Image-guided radiotherapy (IGRT) is expected to reduce the uncertainty of the localization (1, 2).

Frequent displacement of the prostate to the pelvic bony structure has been reported as a problem in the setup of external radiotherapy of prostate cancer for more than 15 years (3, 4). The usefulness of fiducial markers such as radiopaque materials or electromagnetic devices for the assessment of interfraction prostate displacement has also been well established (5–8). Precise repositioning using an IGRT technique with prostate markers has shown to be useful for reducing the margin of the planning target volume (PTV) (5–8). The intrafraction error due to prostate motion was reported to be negligible compared to the interfraction setup error (9).

Recently, however, the intrafraction motion of the prostate gland has emerged as an important limiting factor when considering margins for intensity-modulated radiotherapy (IMRT), which often requires a treatment time longer than that of conventional treatment. Langen *et al.* found that for individual patients, the maximal value of displacements >3 mm at 5 and 10 minutes after initial positioning were 43% and 75%, respectively (10). Litzenberg *et al.* reported that for a skin-based setup with the inclusion of an intrafraction motion, prostate treatments required average margins of 10.2, 12.5, and 8.2 mm in the anterior–posterior (AP), cranial–caudal (CC), and left–right (LR) directions, respectively (11). They suggested that positioning by prostate electromagnetic markers at the start of the treatment fraction reduced these values to 1.8, 5.8, and 7.1 mm, respectively. Most strikingly, they suggested that interportal adjustment would further reduce margins to an average of 1.4, 2.3, and 1.8 mm. (11).

Reprint requests to: Shinichi Shimizu, M.D., Department of Radiology, Hokkaido University School of Medicine, North-15 West-7, Kita-ku, Sapporo, Japan. Tel: (+81) 11-716-1161; Fax: (+81) 11-706-7876; E-mail: sshimizu-rad@umin.ac.jp

Supported by a grant from the Ministry of Education, Science, Sports, and Culture, Japan (No. 21249065 and No. 0158194) and the Japan Society for the Promotion of Science (JSPS) through the "Funding Program for World-Leading Innovative R&D on Science and Technology" (FIRST Program).

Conflict of interest: none.

Received Jan 6, 2011, and in revised form April 14, 2011. Accepted for publication April 19, 2011.

This large difference in the required margin is due to the capability of detection time interval to adjust for intrafraction prostate motion. Kron *et al.* evaluated 184 patients who had two orthogonal x-rays with 3 to 30 min between preimaging and postimaging using an on-board kV imaging system for intrafraction prostate displacement (12). They found that the mean three-dimensional (3D) vector shift between images was 1.7 mm (range, 0–25 mm). There was a large variation in typical shifts between patients (range, 1 ± 1 to 6 ± 2 mm) with no apparent trends throughout the treatment course. They concluded that given the variation between patients, a uniform set of margins for all patients might not be satisfactory when high target doses are to be delivered.

To reduce the intrafraction displacement of the prostate gland during delivery of radiotherapy, we have been using implanted fiducial markers and a real-time tumor-tracking radiotherapy (RTRT) system in IMRT for prostate cancer for 10 years. We have adopted interportal adjustment of the patient table position during IMRT (13). The preliminary clinical results were encouraging (14). In this study, the incidence of table position adjustment required to keep the intrafractional uncertainty within 2.0 mm was investigated. The appropriateness of our approach of keeping the target correctly located below the threshold of displacement using interportal adjustment of the table position will be also discussed.

METHODS AND MATERIALS

In our treatment protocol for prostate cancer, three gold markers 2.0 mm in diameter were inserted into the prostate gland before computed tomography (CT) for treatment planning. The gold markers were inserted into the clinical target volume (CTV) of the prostate gland, one at the apex of the prostate and two others at the left and right of the base of the gland. Computed tomography of the small pelvis was taken with a 1.0-mm slice thickness and 1.0-mm interval with the patient in the supine position on a flat carbon table. Pinnacle3 (Hitachi Medical Co., Tokyo) was used as the 3D radiation treatment planning system (3DRTP). The contours of the prostate gland were defined as the CTV, and the positions of the three fiducial markers were determined on 3DRTP using CT images. The coordinates of the CTV and the three fiducial markers were determined using the 3DRTP. The PTV was determined by a 3D expansion of the CTV with the addition of a 3-mm margin. Then, 70 Gy at a D95 of PTV was delivered with step-and-shoot IMRT in 30 fractions in 30 sessions. Seven ports were used in IMRT, and all seven ports were used in each daily treatment.

The RTRT system consists of a conventional 6-MV or 10-MV linear accelerator, two diagnostic x-ray fluoroscopic systems in the linear accelerator room, image processing units, and an image display unit (originally Mitsubishi; changed to Varian Medical Japan Co., Tokyo) (5, 13).

The actual position of the markers can be visualized during irradiation. The marker position is transferred from 3DRTP and superimposed on the fluoroscopic image on the display unit of the RTRT system. Details of the calculation of the parallel and rotational setup error have already been reported (15). In short, the position of the patient can be corrected by adjusting the patient table position by a remote control bar on the treatment console. When the displacement of the center of gravity of the three markers (DCG) exceeds the threshold, the operator can correct the patient table position using the remote control unit. The threshold used in this study was 2.0 mm in each direction—AP, CC, and LR—thus, if the displacement exceeded 2.0 mm in any direction, the table position was corrected so that the center of gravity of the three markers would be within 0.1 mm of its planned position. Therefore, the length (in millimeters) of the patient table adjustment is equal to the DCG in the body. The table position can be changed in the lateral, vertical, and longitudinal directions within an accuracy of ± 0.1 mm of the specifications. In our previous study on the RTRT data of 123 setups of 5 patients, the random rotational error around the x, y, and z axes in the manual setup was 3.0, 5.1, and 5.0 degrees, respectively. The systematic rotational error around the x, y, and z axes in the manual setup calculated from the 5 patients' data was 3.0, 2.4, and 4.9, respectively (16). On the basis of these data, we calculated the rotational setup error around each axis but intentionally did not correct them in this study.

The RTRT system has several options for the frequency of observation. Our system has the option to gate/stop the treatment if the discrepancy from the previous image is over 2 mm, but we would need to expose a diagnostic x-ray every 0.033 to 0.1 second for this purpose. We decided that it would not be proper to continuously generate diagnostic x-rays during treatment for slow prostate motion. Therefore, we used another option, that of consulting a single exposure at the start of every treatment beam portal and intermittently during the beam delivery. The 3D coordinates of the three gold markers were measured with the RTRT system, and the table position was corrected if the DCG was greater than 2.0 mm. For patients in whom displacement was frequently observed, the coordinates of the three markers were measured two times or more during the delivery of one portal irradiation. The position of the patient table was continuously corrected so as not to diverge from the planned position. The time required from the detection to the adjustment of the displacement was usually less than 1 minute. Thus, the interval between exposures ranged from about 1 minute to 3 minutes.

The length of the table position adjustment after the initial setup during the treatment was stored in the data server of the RTRT system. Using the datasets in the server, we could analyze the incidence and magnitude of the interportal requirement of patient table position adjustment after the initial setup during daily treatment. The incidence should be consistent with the incidence of DCG exceeding the threshold of 2.0 mm during the irradiation for each port.

In this study, datasets of 20 patients consecutively treated between 2004 and 2008 were used to reveal the requirement of interportal patient table position adjustment after the initial setup during daily treatment to keep the accuracy within 2.0 mm. The patient ages ranged from 55 to 76 years, with a median age of 70 years. There were 12, 4, and 4 patients with T1N0M0, T2N0M0, and T3N0M0 disease, respectively. There was no specific regimen for bladder and rectal filling, but patients were instructed to void about 1 hour before the time of daily treatment. The study was approved by the institutional ethical committee, and written informed consent was obtained from all patients before the insertion of the markers.

Statistical analysis was done with JMP 8.0.1(SAS Institute, Cary, NC, USA). Statistical significance was tested by the chi-square test. Analysis was performed after treatment for all patients.

RESULTS

Each patient was treated with 30 sessions, so that datasets of 600 sessions were obtained in total (30 sessions times 20

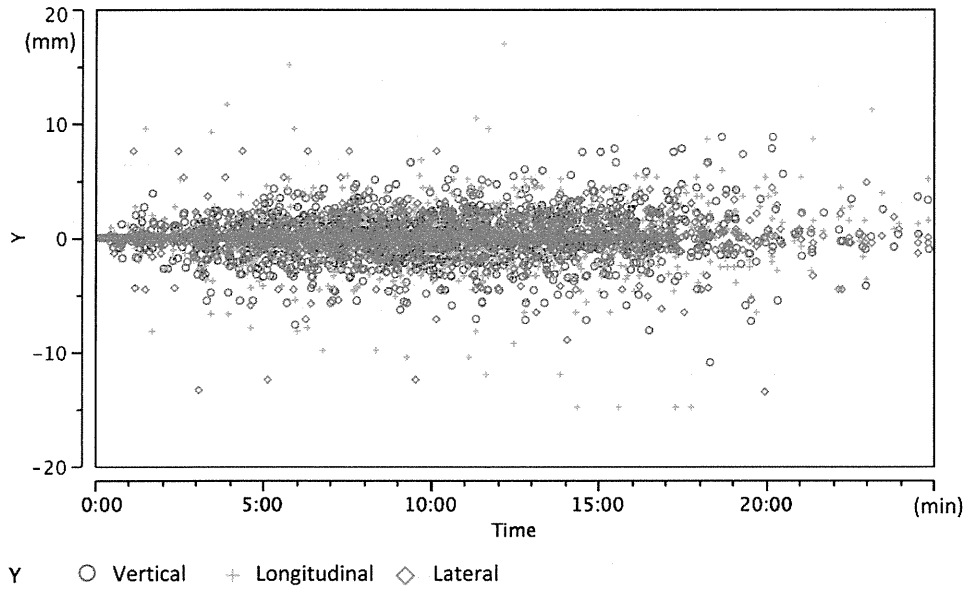

Fig. 1. Displacement of the center of gravity of the three gold markers according to time after initial setup at the start of each treatment day in 20 patients. The x axis shows the time in minutes from the initial setup, and the y axis represents the amount of the displacement in mm for each treatment day. Displacements in the anterior–posterior, Cranial–caudal, and left–right directions are plotted on the same scale.

patients). Datasets of 45 sessions were excluded because of insufficient records or prolonged treatment time caused by the general condition of the patients. Consequently, datasets of 555 sessions were used for the analysis. As a result, 4,541 observation points were obtained from the 20 patients. The average number of observations per patient was 227.1, and that per session was 7.6.

Figure 1 shows the displacement of the center of gravity of the three gold markers according to the time after the initial setup at the start of each treatment day. The x axis shows the time in minutes from the initial setup, and the y axis represents the displacement in millimeters for each treatment day. Displacements in the AP, CC, and LR directions are plotted on the same graph at the same scale. The displacement was sporadically but definitely larger than 2.0 mm during the course of IMRT.

The total incidences of patient table position adjustment after the initial setup during treatment were 465 times in total for 30 sessions in the 20 patients. For 1 patient, the median incidence was 19 times, ranging from six times to 68. The incidences of patient table position adjustment after the initial setup during treatment are shown in Fig. 2. The results show that the incidence of required interportal table position adjustment was as low as 0.5% within the initial 2 minutes, but its accumulated incidence during daily irradiation was not negligible. Details of the incidence of required interportal table position adjustment with 95% confidence intervals are shown in the table. The incidence of table position adjustment was 14.2% in AP, 12.3% in CC, and 5.0% in the LR direction, respectively, at 10 minutes from the initial setup of each treatment. The accumulated incidence of table position adjustment was significantly higher at 10 minutes compared with the incidence at 2 minutes in the AP direction ($p = 0.0033$) and CC direction ($p = 0.0110$) but not in the LR direction ($p = 0.4296$).

Adjustment more than 5 mm was required at least once in 10 minutes in 7 (35%) patients and at some point in the treatment period in 11 (55%) patients of the 20 patients entered in this study. If each patient had some characteristics of prostate motion, we might be able to predict the need for interportal adjustment of the table position. We applied the following criteria arbitrarily to stratify the patients into three categories in this study. If displacement exceeded 5 mm within 10 minutes at least once, the patient was classified into the "large motion" type. Patients who experienced displacement over 5 mm after 10 minutes but not in the initial 10 minutes were classified as the "increasing" type. If displacement over 5 mm did not occur even after 10 minutes, the patient was classified as the "steady" type (Fig. 3). Applying these criteria, there were 7, 4, and 9 patients, respectively, in the groups of "large motion," "increasing," and "steady" type in our series. For each patient, we investigated whether the grouping from the first five fractions placed that patient into the same group as the total 30 fractions. Five of 7 patients with "large motion," 2 of 4 patients with "increasing," and 20 of 9 patients with "steady" type were classified in the same category using the initial five fractions.

DISCUSSION

Recent studies have shown that ultrasound-based systems, in-room CT, in-room kV fluoroscopy, and cone-beam computed tomography are useful in reducing the setup error for a majority of radiation patients (17–20). Our method using fiducial markers and two sets of fluoroscopy was also shown to be useful to reduce setup error compared

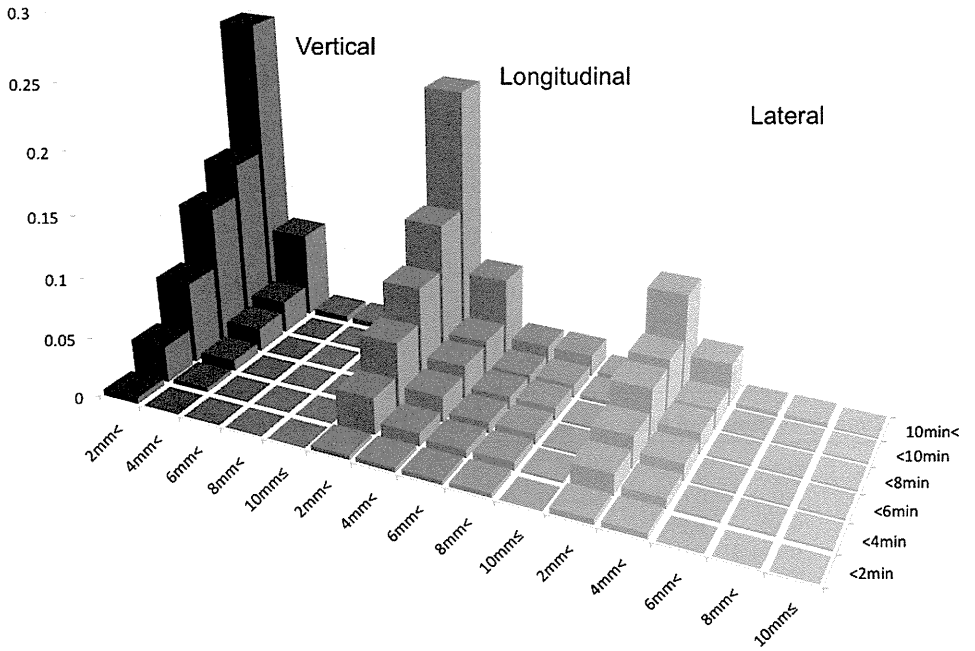

Fig. 2. Incidences of patient table position adjustment after initial setup during the treatment. The length of the table position adjustment was stratified in 2-mm intervals. The incidence of adjustment was stratified in 2-minute intervals after the initial setup. The figure shows the cumulative incidence of displacement at 2, 4, 6, 8, and 10 minutes, and thereafter.

with the skin-based setting (5, 13, 15). In this study, we focused on intrafraction displacement according to treatment time, from the beginning of each treatment session after the daily setup procedure was finished.

The importance of sporadic intrafraction prostate motion has been reported in recent years. Kotte *et al.* analyzed the portal images of 427 patients with Stage T3NxMx prostate carcinoma who received IMRT combined with position verification with fiducial markers with the irradiation time of 5 to 7 minutes (21). In 66% of the treatment fractions, a motion outside the range of 2 mm was observed, with 28% outside the range of 3 mm. They found that intrafraction motion caused position uncertainty with systematic errors (Σ) to <0.6 mm and random errors (σ) to <0.9 mm, and suggested a lower limit of 2 mm for margins with online position correction at the start of irradiation. We also found that the intrafraction displacement was usually as small as 2 mm on average during the initial 2 minutes. However, the displacement became larger according to the elapsed treatment time after the start of radiotherapy in our series. A similar trend was observed in recent studies in which patients had treatment times longer than 5 minutes (10, 22). Thus, among patients expected to have radiotherapy lasting longer than 2 minutes, careful observation during the delivery of radiotherapy with interportal adjustment may be useful for a small but definite number of patients.

In this study, interportal adjustment of the patient table combined with the use of three implanted markers and two sets of fluoroscopy was shown to be effective in maintaining the accuracy of the prostate position. The benefit of quick estimation of prostate displacement using the RTRT system was apparent, considering the minimal elongation of the treatment time. Similar midsession adjustment of table position has been reported using a robotic linear accelerator for hypofractionated radiotherapy of the prostate, which often requires 50 to 70 minutes for one treatment session (23). Those authors found that when sporadic prostate movements greater than 5 mm were present in any one direction, significant changes in the dose–volume histogram could be detected. Compared with their stereotactic hypofractionated radiotherapy, our protocol has a shorter daily treatment time. However, step-and-shoot IMRT often requires 10 minutes, which is still long enough for an intrafraction prostate motion larger than 5 mm to occur.

Litzenberg *et al.* have estimated that midsession adjustment would reduce margins to an average of 1.4, 2.3, and 1.8 mm (11). Their results are consistent with the study by Nederveen *et al.* suggesting that a 1- to 2-mm margin is sufficient for intrafraction displacement providing that position verification is performed at time intervals of 2 to 3 min (7). We confirmed that the margin for prostate motion can be significantly reduced by our interportal adjustment technique. The margin for internal organ motion was kept at 2 mm for each direction in our protocol.

It is still not certain whether we should use real-time tracking of the prostate markers during the delivery of radiotherapy as RTRT for lung cancers (24) and permit irradiation only when the fiducial markers are within the gating window. Litzenberg *et al.* suggested that 2 of their 11 patients would have benefited from continuous target tracking and

Table. Means and 95% confidence intervals of the distribution of incidence of prostate displacement

Vertical	Anterior	~2 mm	~4 mm	~6 mm	~8 mm	~10 mm	Posterior	~2 mm	~4 mm	~6 mm	~8 mm	~10 mm
	<2 min	0.0%	0.0%	0.0%	0.0%	0.0%	<2 min	0.5%	0.0%	0.0%	0.0%	0.0%
		0.0–0.7	0.0–0.7	0.0–0.7	0.0–0.7	0.0–0.7		0.2–1.6	0.0–0.7	0.0–0.7	0.0–0.7	0.0–0.7
	<4 min	1.8%	0.4%	0.0%	0.0%	0.0%	<4 min	1.3%	0.0%	0.0%	0.0%	0.0%
		1.0–3.3	0.1–1.3	0.0–0.7	0.0–0.7	0.0–0.7		0.6–2.6	0.0–0.7	0.0–0.7	0.0–0.7	0.0–0.7
	<6 min	3.8%	0.5%	0.0%	0.0%	0.0%	<6 min	3.1%	0.4%	0.0%	0.0%	0.0%
		2.5–5.7	0.2–1.6	0.0–0.7	0.0–0.7	0.0–0.7		1.9–4.9	0.1–1.3	0.0–0.7	0.0–0.7	0.0–0.7
	<8 min	6.1%	1.3%	0.0%	0.0%	0.0%	<8 min	5.6%	0.7%	0.0%	0.0%	0.0%
		4.4–8.4	0.6–2.6	0.0–0.7	0.0–0.7	0.0–0.7		4.0–7.8	0.3–1.8	0.0–0.7	0.0–0.7	0.0–0.7
	<10 min	7.6%	1.6%	0.0%	0.0%	0.0%	<10 min	6.7%	1.1%	0.0%	0.0%	0.0%
		5.6–10.1	0.9–3.1	0.0–0.7	0.0–0.7	0.0–0.7		4.9–9.1	0.5–2.3	0.0–0.7	0.0–0.7	0.0–0.7
	>10 min	11.9%	3.4%	0.4%	0.4%	0.2%	>10 min	13.0%	3.8%	0.2%	0.2%	0.0%
		9.5–14.9	2.2–5.3	0.1–1.3	0.1–1.3	0.0–1.0		10.4–16.0	2.5–5.7	0.0–1.0	0.0–1.0	0.0–0.7
Longitudinal	**Cranial**	**~2 mm**	**~4 mm**	**~6 mm**	**~8 mm**	**~10 mm**	**Caudal**	**~2 mm**	**~4 mm**	**~6 mm**	**~8 mm**	**~10 mm**
	<2 min	0.2%	0.2%	0.2%	0.2%	0.0%	<2 min	0.4%	0.2%	0.2%	0.2%	0.0%
		0.0–0.7	0.0–1.0	0.0–1.0	0.0–1.0	0.0–0.7		0.1–1.3	0.0–1.0	0.0–1.0	0.0–1.0	0.0–0.7
	<4 min	1.8%	0.4%	0.2%	0.2%	0.0%	<4 min	1.3%	0.7%	0.5%	0.5%	0.2%
		1.0–3.3	0.1–1.3	0.0–1.0	0.0–1.0	0.0–0.7		0.6–2.6	0.3–1.8	0.2–1.6	0.2–1.6	0.0–1.0
	<6 min	3.2%	1.1%	0.2%	0.2%	0.0%	<6 min	2.5%	1.1%	0.7%	0.7%	0.2%
		2.1–5.1	0.5–2.3	0.0–1.0	0.0–1.0	0.0–07		1.5–4.2	0.5–2.3	0.3–1.8	0.3–1.8	0.0–1.0
	<8 min	4.7%	1.4%	0.4%	0.4%	0.0%	<8 min	4.0%	1.4%	0.7%	0.7%	0.2%
		3.2–6.8	0.7–2.8	0.1–1.3	0.1–1.3	0.0–0.7		2.6–5.9	0.7–2.8	0.3–1.8	0.3–1.8	0.0–1.0
	<10 min	7.2%	1.8%	0.4%	0.4%	0.2%	<10 min	5.0%	1.4%	0.7%	0.7%	0.2%
		5.6–10.1	0.9–3.1	0.0–0.7	0.0–0.7	0.0–0.7		3.5–7.2	0.7–2.8	0.3–1.8	0.3–1.8	0.0–1.0
	>10 min	10.5%	2.7%	0.5%	0.5%	0.2%	>10 min	11.4%	4.1%	1.3%	1.3%	0.4%
		8.2–13.3	1.6–4.4	0.2–1.6	0.2–1.6	0.0–1.0		9.0–14.3	2.8–6.1	0.6–2.6	0.6–2.6	0.1–1.3
Lateral	**Left**	**~2 mm**	**~4 mm**	**~6 mm**	**~8 mm**	**~10 mm**	**Right**	**~2 mm**	**~4 mm**	**~6 mm**	**~8 mm**	**~10 mm**
	<2 min	0.4%	0.4%	0.0%	0.0%	0.0%	<2 min	0.2%	0.2%	0.0%	0.0%	0.0%
		0.1–1.3	0.1–1.3	0.0–0.7	0.0–0.7	0.0–0.7		0.0–1.0	0.0–1.0	0.0–0.7	0.0–0.7	0.0–0.7
	<4 min	0.9%	0.5%	0.2%	0.2%	0.2%	<4 min	0.9%	0.4%	0.0%	0.0%	0.0%
		0.4–2.1	0.2–1.6	0.0–1.0	0.0–1.0	0.0–1.0		0.4–2.1	0.1–1.3	0.0–0.7	0.0–0.7	0.0–0.7
	<6 min	1.6%	1.1%	0.2%	0.2%	0.2%	<6 min	1.1%	0.4%	0.0%	0.0%	0.0%
		0.9–3.1	0.5–2.3	0.0–1.0	0.0–1.0	0.0–1.0		0.5–2.3	0.1–1.3	0.0–0.7	0.0–0.7	0.0–0.7
	<8 min	2.3%	1.4%	0.2%	0.2%	0.2%	<8 min	2.2%	0.4%	0.0%	0.0%	0.0%
		1.4–4.0	0.7–2.8	0.0–1.0	0.0–1.0	0.0–1.0		1.2–3.7	0.1–1.3	0.0–0.7	0.0–0.7	0.0–0.7
	<10 min	2.5%	1.4%	0.2%	0.2%	0.2%	<10 min	2.5%	0.4%	0.0%	0.0%	0.0%
		1.5–4.2	0.7–2.8	0.0–1.0	0.0–1.0	0.0–1.0		1.5–4.2	0.1–1.3	0.0–0.7	0.0–0.7	0.0–0.7
	>10 min	3.8%	2.5%	0.4%	0.4%	0.2%	>10 min	4.9%	1.1%	0.0%	0.0%	0.0%
		2.5–5.7	1.5–4.2	0.1–1.3	0.1–1.3	0.0–1.0		3.4–7.0	0.5–2.3	0.0–0.7	0.0–0.7	0.0–0.7

Each cell is gray-coded according to probability: ≤0.5% = white; 0.5–5% = light gray; ≥5% = gray.

threshold-based intervention from their analysis of intrafraction organ motion (11). Nederveen *et al.* found marker displacements as large as 9.5 mm in one fraction and suggested the need for frequent verification in some patients (7). We also observed several patients other than the 20 patients in this study for whom the prostate position was so unstable that real-time tracking of the marker and gated irradiation was used. The amount of motion of the prostate is far different than that from respiratory motion, probably because of the motion of gas in the rectum. By contrast, a large proportion of patients experienced not so large displacement during their irradiation. Appropriate criteria are required to use real-time tracking of the marker and threshold-based intervention.

We identified at least three types of patients in terms of internal prostate motion. If we could predict which patients are steady types, we would not require any online monitoring of the prostate motion during delivery of their radiotherapy. Likewise, if a patient could be preidentified as a large-motion type, frequent monitoring or even real-time tracking of the marker position could be used to reduce the risk of adverse effects and local relapse. For patients in the increasing-motion type, modest monitoring of the marker would be appropriate. In our preliminary analysis in this study, we found that we could detect patients with large motion with considerable probability from the observation of the first five fractions. However, the distinction between the increasing and steady types seemed to be difficult. These

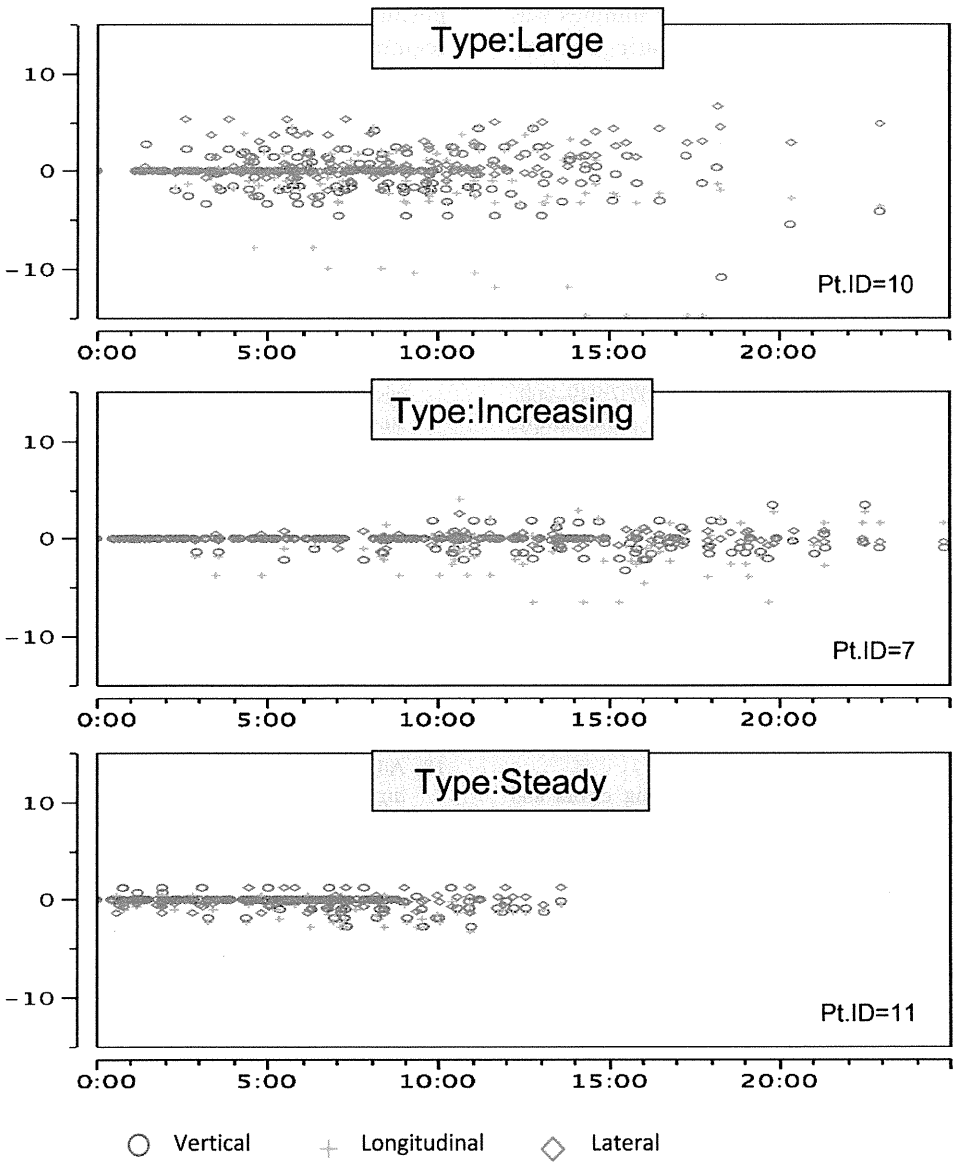

Fig. 3. Displacement of the center of gravity of the three markers in 3 patients who were stratified into "large motion," "increasing," and "steady" types, respectively.

types were arbitrarily determined in this study, and the distinction requires further analysis.

The shortcomings of this study are as follows. First, frequent observation of the markers using diagnostic fluoroscopy increases the patients' radiation exposure. However, given that a couple of orthogonal x-ray static images are sufficient to measure the displacement of the prostate gland in the interportal adjustment, the total amount of exposure is estimated to be negligible with seven-portal IMRT. Making position corrections using the RTRT system, as with other IGRT devices, can reduce the CTV–PTV margin, which might otherwise exceed that actually required, and therefore reduce the dose around the CTV (25).

Second, a treatment time of more than 10 minutes for IMRT may be too long in the era of high-dose-rate external radiotherapy. Our results may be regarded as data to support the appropriateness of developing a high-dose-rate external radiotherapy system with a short treatment time. Aznar *et al.* reported that when the volumetric modulated arc therapy was used to treat prostate cancer patients, it required less than 2 minutes of beam-on time per treatment (26). In our study, within 2 minutes after initial patient setup for daily treatment, the movement of the prostate was limited. Thus, a faster treatment is suitable for avoiding excursion or drifts of the target when an intrafraction adjustment is not used. On the other hand, spot scanning particle beam therapy and intensity-modulated proton beam therapy are now becoming available to reduce the low-dose large-area irradiation in IMRT and neutron contamination in conventional proton therapy. These new techniques would require more than several minutes with the expectation for higher accuracy in patient positioning. Our results suggest that these high-tech methods should match the requirement for interportal adjustment of the treatment position to accomplish their goal.

In conclusion, the displacement during 10 minutes was significantly larger than the displacement during the initial 2 minutes. The probability of displacement of more than 2.0 mm is under 0.5% in the initial 2 minutes in the AP, CC, and LR directions, respectively. However, without interportal adjustment of the patient table, intrafraction displacement may not be negligible in treatments longer than 2 minutes. Interportal adjustment of table position during the 10 minutes after initial setup was required in more than 10% of portal irradiations to maintain treatment accuracy within 2.0 mm. The implantation of three fiducial markers and interportal adjustment of the patient table with the RTRT system was shown to be useful in maintaining the intrafraction displacement within the predetermined range of 2.0 mm for localized prostate cancer.

REFERENCES

1. Verellen D, De Ridder M, Linthout N, *et al.* Innovations in image-guided radiotherapy. *Nat Rev Cancer* 2007;7:949–960.
2. Shirato H. Organ motion in image-guided radiotherapy: Lessons from real-time tumor-tracking radiotherapy. *Int J Clin Oncol* 2007;12:8–16.
3. van Herk M, Bruce A, Guus Kroes AP, *et al.* Quantification of organ motion during conformal radiotherapy of the prostate by three dimensional image registration. *Int J Radiol Oncol Biol Phys* 1995;33:1311–1320.
4. Crook JM, Raymond Y, Salhani D, *et al.* Prostate motion during standard radiotherapy as assessed by fiducial markers. *Radiother Oncol* 1995;37:35–42.
5. Shimizu S, Shirato H, Kitamura K, *et al.* Use of an implanted marker and real-time tracking of the marker for the positioning of prostate and bladder cancers. *Int J Radiat Oncol Biol Phys* 2000;48:1591–1597.
6. Wu J, Haycocks T, Alasti H, *et al.* Positioning errors and prostate motion during conformal prostate radiotherapy using on-line isocentre set-up verification and implanted prostate markers. *Radiother Oncol* 2001;61:127–133.
7. Nederveen AJ, van der heide UA, van Moorselaar RJ, *et al.* Measurements and clinical consequences of prostate motion during a radiotherapy fraction. *Int J Radiat Oncol Biol Phys* 2002;53:206–214.
8. Schallenkamp JM, Herman MG, Kruse JJ, *et al.* Prostate position relative to pelvic body anatomy based on intraprostatic gold markers and electronic portal imaging. *Int J Radiat Oncol Biol Phys* 2005;63:800–811.
9. Huang E, Dong L, Chandra A, *et al.* Intrafraction prostate motion during IMRT for prostate cancer. *Int J Radiat Oncol Biolo Phys* 2002;53:261–268.
10. Langen KM, Willoughby TR, Meeks SL, *et al.* Observations on real-time prostate gland motion using electromagnetic tracking. *Int J Radiat Oncol Biol Phys* 2008;71:1084–1090.
11. Litzenberg DW, Balter JM, Hadley SW, *et al.* Influence of intrafraction motion on margins for prostate radiotherapy. *Int J Radiat Oncol Biol Phys* 2006;65:548–553.
12. Kron T, Thomas J, Fox C, *et al.* Intra-fraction prostate displacement in radiotherapy estimated from pre- and post-treatment imaging of patients with implanted fiducial markers. *Radiother Oncol* 2010;95:191–197.
13. Shirato H, Oita M, Fujita K, *et al.* Three-dimensional conformal setup (3D-CSU) of patients using the coordinate system provided by three internal fiducial markers and two orthogonal diagnostic X-ray systems in the treatment room. *Int J Radiat Oncol Biol Phys* 2004;60:607–612.
14. Kitamura K, Shirato H, Shinohara N. Reduction in acute morbidity using hypofractionated intensity-modulated radiation therapy assisted with a fluoroscopic real-time tumor-tracking system for prostate cancer: Preliminary results of a phase I/II study. *Cancer J* 2003;9:268–276.
15. Shirato H, Shimizu S, Kunieda T, *et al.* Physical aspects of a real-time tumor-tracking system for gated radiotherapy. *Int J Radiat Oncol Biol Phys* 2000;48:1187–1195.
16. Fujita K, Shirato H, Kitamura K, *et al.* Three-dimensional conformal set-up of prostate cancer by adjustment of actual clinical target volume (CTV) to virtual CTV using three fiducial markers and fluoroscopic real-time tracking system. *Int J Radiat Oncol Biol Phys* 2001;51:384.
17. Wong J, Grimm L, Uematsu M, *et al.* Image-guided radiotherapy for prostate cancer by CT-linear accelerator combination: Prostate movements and dosimetric considerations. *Int J Radiat Oncol Biol Phys* 2005;61:561–569.
18. Adamson J, Wu Q. Prostate intrafraction motion evaluation using kV fluoroscopy during treatment delivery: A feasibility and accuracy study. *Med Phys* 2008;35:1793–1806.
19. Adamson J, Wu Q. Prostate intrafraction motion assessed by simultaneous kilovoltage fluoroscopy at megavoltage delivery I: Clinical observations and pattern analysis. *Int J Radiat Oncol Biol Phys* 2010;78:1563–1570.
20. Pinkawa M, Pursch-Lee M, Asadpour B, *et al.* Image-guided radiotherapy for prostate cancer: Implementation of ultrasound-based prostate localization for the analysis of inter- and intrafraction organ motion. *Strahlenther Onkol* 2008;184:679–685.
21. Kotte A, Hofman P, Lagendijk J, *et al.* Intrafraction motion of the prostate during external-beam radiation therapy: Analysis of 427 patients with implanted fiducial markers. *Int J Radiat Oncol Biol Phys* 2007;69:419–425.
22. Xie Y, Djajaputra D, King CR, *et al.* Intrafractional motion of the prostate during hypofractionated radiotherapy. *Int J Radiat Oncol Biol Phys* 2008;72:236–246.
23. Hossain S, Xia P, Chuang C, *et al.* Simulated real time image guided intrafraction tracking-delivery for hypofractionated prostate IMRT. *Med Phys* 2008;35(9):4041–4048.
24. Onimaru R, Fujino M, Yamazaki K, *et al.* Steep dose-response relationship for stage I non-small-cell lung cancer using hypofractionated high-dose irradiation by real-time tumor-tracking radiotherapy. *Int J Radiat Oncol Biol Phys* 2008; 70:374–381.
25. Kron T, Wong J, Rolfo A, *et al.* Adaptive radiotherapy for bladder cancer reduces integral dose despite daily volumetric imaging. *Radiother Oncol* 2010;97: 485–47.
26. Aznar MC, Petersen PM, Logadottir A, *et al.* Rotational radiotherapy for prostate cancer in clinical practice. *Radiother Oncol* 2010;97:480–484.

Dynamic gating window for compensation of baseline shift in respiratory-gated radiation therapy

Eric W. Pepin[a)]
School of Health Sciences, Purdue University, West Lafayette, Indiana 47907

Huanmei Wu
Purdue School of Engineering Technology, IUPUI, Indianapolis, Indiana 46202

Hiroki Shirato
Hokkaido University School of Medicine, Sapporo, Japan 060-8638

(Received 19 October 2010; revised 20 January 2011; accepted for publication 29 January 2011; published 11 March 2011)

Purpose: To analyze and evaluate the necessity and use of dynamic gating techniques for compensation of baseline shift during respiratory-gated radiation therapy of lung tumors.
Methods: Motion tracking data from 30 lung tumors over 592 treatment fractions were analyzed for baseline shift. The finite state model (FSM) was used to identify the end-of-exhale (EOE) breathing phase throughout each treatment fraction. Using duty cycle as an evaluation metric, several methods of end-of-exhale dynamic gating were compared: An *a posteriori* ideal gating window, a predictive trend-line-based gating window, and a predictive weighted point-based gating window. These methods were evaluated for each of several gating window types: Superior/inferior (SI) gating, anterior/posterior beam, lateral beam, and 3D gating.
Results: In the absence of dynamic gating techniques, SI gating gave a 39.6% duty cycle. The ideal SI gating window yielded a 41.5% duty cycle. The weight-based method of dynamic SI gating yielded a duty cycle of 36.2%. The trend-line-based method yielded a duty cycle of 34.0%.
Conclusions: Dynamic gating was not broadly beneficial due to a breakdown of the FSM's ability to identify the EOE phase. When the EOE phase was well defined, dynamic gating showed an improvement over static-window gating. © *2011 American Association of Physicists in Medicine.* [DOI: 10.1118/1.3556588]

Key words: lung cancer, respiratory motion, respiratory gating, baseline shift

I. INTRODUCTION

It has been well documented that respiratory motion creates an uncertainty in the targeting of radiotherapy for lung tumors[1] and that this motion can be greater than 1–5 cm,[2–7] though smaller in medial and apical tumors.[8] This uncertainty brings about a need for larger treatment margins in conventional radiation therapy,[6] usually 1–2 cm (Refs. 9 and 10) and as high has 3.1 cm.[11] Respiratory gating is an advanced image guided radiation treatment approach to compensate tumor motion induced by patient respiration. The beam is on only when the tumor is in a certain predefined region, i.e., *the gating window*. Gating has been in use since the late 1980s.[12,13] Its primary application is for lung cancer, but applications have included liver[7] and breast cancer.[14] Previous studies have shown that respiratory gating can reduce treatment margin up to 36% in the superior/inferior (SI) direction, giving margins as small as 3 mm.[4,11,15–17] However, respiratory gating increases the total treatment time of a patient.[18]

Based on gating window determination, there are two common gating approaches: Phase-based gating and amplitude gating. In phase-based gating, the gating window is set to be some percent of the breathing cycle, effectively fixing the duty cycle.[19] In amplitude-based gating, the window is a fixed width about some window center corresponding to tumor motion in the SI, lateral (LAT), and/or anterior/posterior (AP) directions.[18–21] Studies have been done with gating windows ranging from 2.5 to 12.5 mm wide[18] and by defining the window based on displacement percentiles.[21] One study showed little difference between phase-based and amplitude-based gating.[19] Gating windows are often defined about the most extreme positions in the breathing cycle:[9] The end-of-exhalation (EOE) and the end-of-inhalation (EOI). EOE is chosen more often[7,10,15–17,20,22–24] and is more effective[4] because EOE has longer duration and slower tumor motion.[8,9,16,25] In addition, the position of the EOE window is more reproducible.[3,19,20,25,26] EOI gating is often used with a breath-hold technique (deep-inspiration breath-hold) to increase reproducibility and stability.[5,26,27] EOI gating has the advantage of lower lung toxicity to surrounding normal tissue than EOE gating;[2,8,9,19,25,26] however, EOI gating has more residual motion than EOE gating.[19]

One metric for evaluating respiratory gating is the duty cycle, which is the fraction of total treatment time during which radiation is being delivered. In fixed-duty cycle experiments, the efficacy of duty cycles ranging from 20% to 50% have been studied.[1,9,11,15,21,22,24,26–28] In experiments with fixed gating windows, duty cycles ranging from 12.2% to 69% have been seen.[4,7,8,17,20] Various studies have sought to improve the performance of respiratory gating by provid-

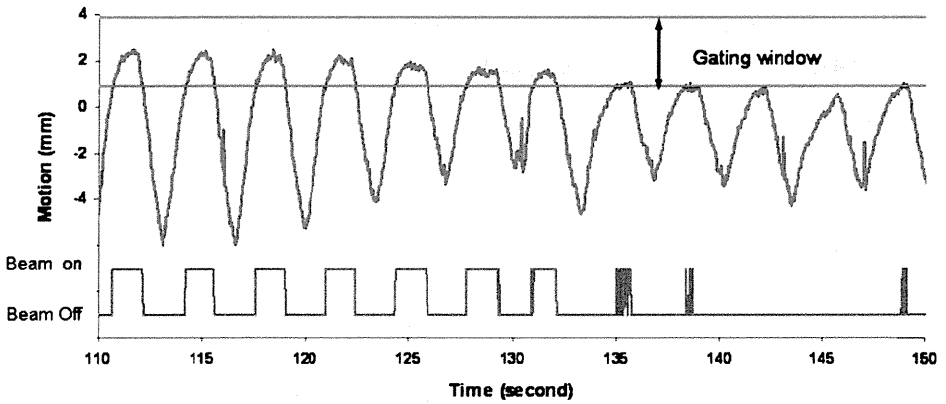

FIG. 1. Fixed amplitude-based gating window for tumor motion with baseline shift and the corresponding beam on/off signal over time.

ing audio or visual coaching to patients so as to increase the reproducibility and stability of their breathing patterns, especially while the tumor is in the gating window.[3,7,9] It has been found that EOI gating with audio coaching is equivalent to EOE gating when both techniques have a fixed 30% duty cycle.[19]

Respiratory motion is patient-specific and there are changes over time in motion amplitude, respiratory period, and baseline location from one breathing cycle to another. In addition, there is noise signal, including random spike noise generated from the tracking system and noise from cardiac motion.[29] Figure 1 illustrates the superior-inferior motion trace of a lung tumor tracked based on an internal implanted fiducial marker. Phase-based gating is vulnerable to duty cycle fluctuations and amplitude variation, which will decrease the effectiveness of the treatment and potentially increase false beam on time, such as during 135–150 s in Fig. 1. In a phase-based gating scenario, the beam will be on even though the tumor is not in the gating window. The amplitude-based gating can detect the motion changes; however, the gating duty cycle will be low and will result in much longer treatment time, especially with baseline shift, as demonstrated in Fig. 1. In addition, noise in the motion signal can cause frequent beam toggling, especially if the gating window is not appropriately set, as shown in the latter portion of Fig. 1.

It has been recommended to account for baseline shift when respiratory gating, i.e., a dynamic window center.[14] However, only limited work has been done to improve duty cycles by adjusting the gating window.[20] In this work, we present several methods of dynamic gating for real-time baseline shift compensation and an analysis of their efficacy.

II. METHODS AND MATERIALS

II.A. Materials

This study used the 3D motion of implanted gold fiducials in 30 lung tumors during 592 radiotherapy fractions tracked using real-time fluoroscopy at a rate of 30 Hz by Hokkaido University.[30] Tumor fiducials were tracked with four orthogonal fluoroscopes during individual treatment fractions, generating tuples of the form (t,x,y,z), where x is LAT position, y is SI position, and z is AP position. The average amplitude of tumor motion for each treatment fraction in three dimensions was 13.9 mm (σ=8.2) and the average baseline drift was 6.6 mm (σ=9.2) in the LAT direction, 9.6 mm (σ=10.3) in the SI direction, and 9.1 mm (σ=11.8) in the AP direction. The tumors are considered as solid and nondeformable tumors. If only translational motion is considered, the motion trajectory represents the motion of each voxel in the tumor and the GTV motion.

II.B. Methods

II.B.1. Motion data preprocessing

The motion data were classified using the finite state model (FSM) developed by Wu.[31] The FSM is a real-time algorithm for classifying the breathing state of a motion data point from a moving lung tumor. In the FSM, a data point is classified in one of four breathing states: Exhale, EOE, inhale, and irregular.

II.B.2. Gating window definition

The size of the gating window can be determined in different ways. A smaller gating window will reduce radiation dose to surrounding healthy tissue and critical structures, yet result in lower gating duty cycle, longer treatment duration, and more beam on/off changes. A larger gating window would result in higher duty cycle, yet increased treatment margins. In practice, the gating window size is decided based on the patient-specific respiratory motion patterns and depends on motion stabilities, amplitude, tumor volume, and other information. For this study, gating window sizes of 3 and 5 mm are simulated and compared. A fixed gating window was defined as a 3 or 5 mm spatial window centered on the average tumor position during one or more complete EOE phases, as the EOE state has relative small motion. Four different gating windows were investigated.

- Gating window based on SI position: The gating window was a 1.5 or 2.5 mm expansion for the 3 or 5 mm

gating window, respectively, in each of the superior/inferior directions about the average position of the tumor in the EOE phase.

- Gating window based on AP beam: The gating window was a 1.5 or 2.5 mm expansion in each direction perpendicular to an AP beam, i.e., superior, inferior, right, and left.
- Gating window based on LAT beam: The gating window was a 1.5 or 2.5 mm expansion in each direction perpendicular to a LAT beam, i.e., superior, inferior, anterior, and posterior.
- Gating window based on 3D position: The gating window was a 1.5 or 2.5 mm expansion in each anatomic direction, i.e., superior, inferior, right, left, anterior, and posterior.

II.B.3. Gating window position determination

Three different methods were used to determine how to center the gating window.

- The static gating window center was the average tumor position during the first three EOE phases of the treatment fraction.
- The ideal gating window had gating windows determined *a posteriori* for each EOE phase and placed on the center of each EOE phase.
- Several types of dynamic gating windows had the center of the window changed upon leaving each EOE phase.

II.B.4. Dynamic gating algorithms

Two methods of changing the gating window center were evaluated.

- In the weighted-center method, the average tumor position for each of the previous three EOE phases was considered as the vector triples (x_1,y_1,z_1), (x_2,y_2,z_2), and (x_3,y_3,z_3). The window center was calculated as a weighted average of the vector triples

$$w_1(x_1,y_1,z_1)+w_2(x_2,y_2,z_2)+w_3(x_3,y_3,z_3)$$

where $0\leq w_i\leq 1$, $w_1+w_2+w_3=1$, and $w_1=n\cdot 0.05, n\in Z_{20}$.

All combinations of w_1, w_2, and w_3 were considered and the duty cycle for each combination was calculated for each treatment fraction. For each fraction, the weighting combinations giving the ten largest duty cycles were recorded. Three-dimensional histograms were made showing the number of times each weighting combination was considered favorable using scatter3 in MATLAB (MATLAB® The MathWorks, Natick, MA).

- In the trend-line method, the gating window center was calculated using the slope of a linear regression line fit to the average tumor position of each of several previous EOE phases. This method was evaluated considering the previous two, three, four, and five EOE phases. The window center was calculated by extending the trend-line from its calculated path. N.B.: The trend-line method for three previous EOE phases is a special case of the weighted-center method in which $w_1=w_2=w_3$.

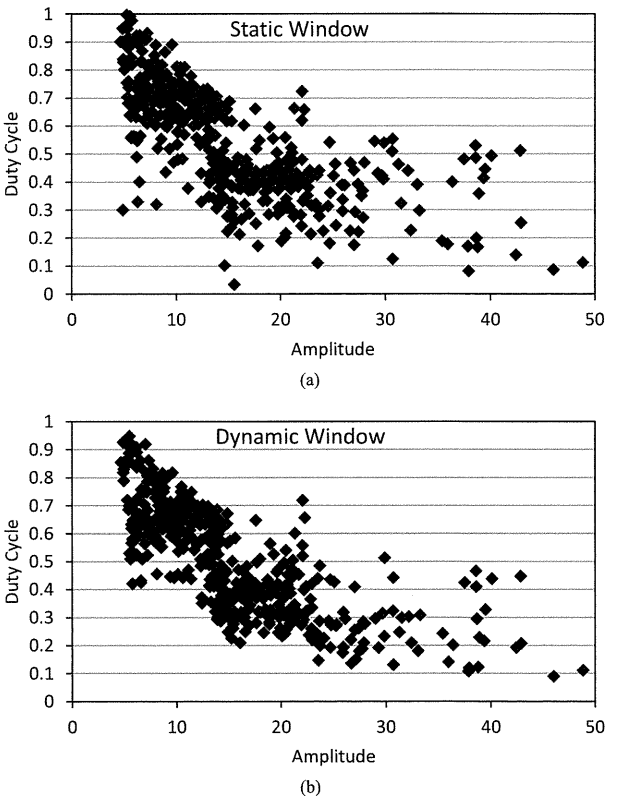

FIG. 2. The relationships of duty cycle and amplitude for each fraction of (a) static gating and (b) dynamic gating, where the gating window size is 5 mm

For each gating window method, the duty cycle was calculated as the fraction of total tracking time that the tumor was located within the gating window.

III. RESULTS

For a 3 mm gating window size, the static-window gating method gave an average duty cycle of 39.6% (σ=17.6%) for a SI gate. The ideal-window gating method gave a significantly larger average duty cycle of 41.5% (σ=16.0%) for a SI gate ($p<0.001$). For the 3D window, the average duty cycle improvement was 4.3% when comparing the ideal window to the static window. Similarly, this improvement was 2.6% for the AP beam and 4.0% for the LAT beam. The analysis was repeated with a 5 mm gating window, the comparative results were unchanged, with duty cycles being increased 12%–14% in all cases. The relationships between the duty cycle and the amplitude (averaged over a treatment fraction) are compared and illustrated in Fig. 2. The scattered plots showed that for fractions with small amplitude and/or low duty cycle, there is more increase of duty cycle from static gating to dynamic gating. This effect was more pronounced with the 5 mm gating window.

The remaining results are presented based on the 3 mm gating window. The weight-based method of dynamic gating

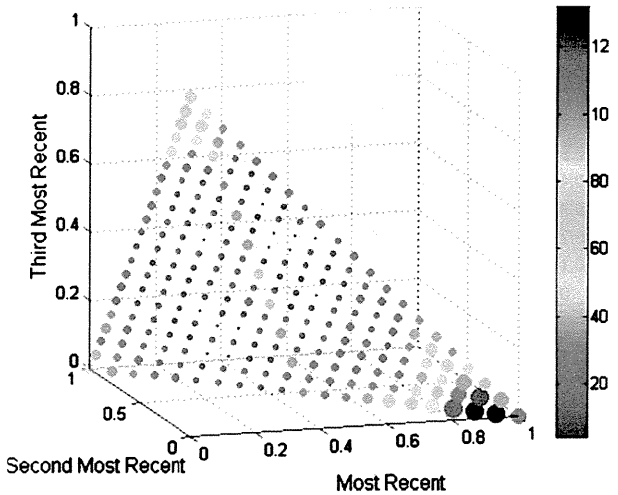

FIG. 3. Histogram showing favorability of weighting combinations for a gating window determined only by considering SI position. The size/color of each marker indicates the favorability of that combination. The histograms for AP, LAT, and 3D beams were similar.

performed best when the most recent EOE phase was given a weighting of at least 0.85 (see Fig. 3). Each fraction was evaluated for all weighting combinations in which w_1 was at least 0.85. The average duty cycle for all fractions shows little variability over the set of weighting combinations for a SI window (36.0%, σ=0.3%). It was also determined how many fractions, at each weighting combination, had duty cycles greater than the static-window case. For a SI gating window, these combinations produced a higher duty cycle in 25%–28% of fractions, with the most benefit occurring with the weighting combination $\langle 0.9, 0.05, 0.05\rangle$: 29%–33% of fractions saw benefits for an AP gating window, with the most benefit from $\langle 0.95, 0.05, 0\rangle$; 34%–39% of fractions saw benefits for a LAT gating window, with the most benefit from $\langle 0.95, 0.05, 0\rangle$; and 35%–40% of fractions saw benefits for a 3D gating window, with the most benefit from $\langle 0.95, 0.05, 0\rangle$.

The trend-line method of dynamic gating showed increasing duty cycle with more EOE phase averages considered in the trend-line from two to four (see Fig. 4). This increase was significant when comparing four EOE phase averages in the trend-line compared to only two for all gating window types ($p<0.03$). Including five EOE phases gave slightly lower duty cycles when compared to four EOE phases; however, this decline was not significant ($p>0.9$).

The results for all methods and window types are summarized in Table I.

TABLE I. Comparison of duty cycles for each type of gating window and method of gating. The duty cycles given for the weighted window are those for the highest performing weighting combination for each window type.

Method	SI DC (%)	AP DC (%)	LAT DC (%)	3D DC (%)
Static window	39.6	36.0	31.0	29.3
Ideal window	41.5	38.6	35.0	33.6
Weighted window	36.2	33.3	29.4	28.1
Trend-line window (n=4)	34.0	30.1	26.6	25.1

IV. DISCUSSION

It was somewhat unexpected that the overall performance over the 30 patients of the real-time dynamic gating methods did not outperform a static window. This led to an investigation of individual tumors and whether a particular gating method consistently produced an increase in the duty cycle during the treatment of particular tumors. The investigation found that tumor motion behavior and motion patterns have great influence on the gating duty cycle. Not all 30 tumors exhibited a significant baseline shift over time and as such, the advantage of dynamic gating did not show. In practice, it may be beneficial to consider the amplitude of tumor motion when fixing the width of the gating window.

For some tumors' motion traces, there are distinctive changes in behavior between the IN, EX, and EOE states. The FSM can easily identify the unambiguous EOE phases as they are distinct from the other breathing phases (Fig. 5). Baseline shift in these motion patterns will benefit more from dynamic gating, as shown in Fig. 6. However, for some tumors, their motion trajectories do not have a prominent EOE stage, resulting in a motion trace that consists of IN and EX states, as shown in Fig. 7. Tumors with this type of motion are not suitable for gated treatment in the first place as it will lead to low duty cycle. In addition, the EOE state of the FSM

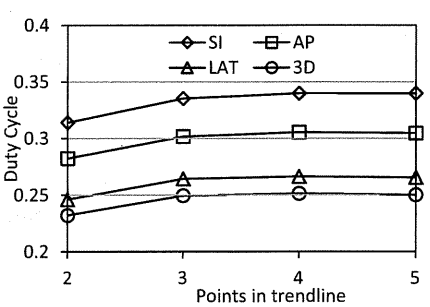

FIG. 4. Average duty cycle for trend-line-based dynamic gating for each window type and number of points in the trend-line.

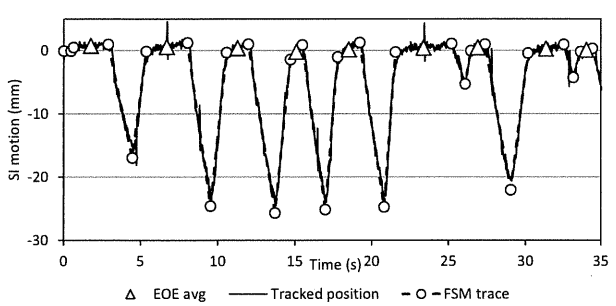

FIG. 5. Example of breathing pattern with well differentiated FSM transitions.

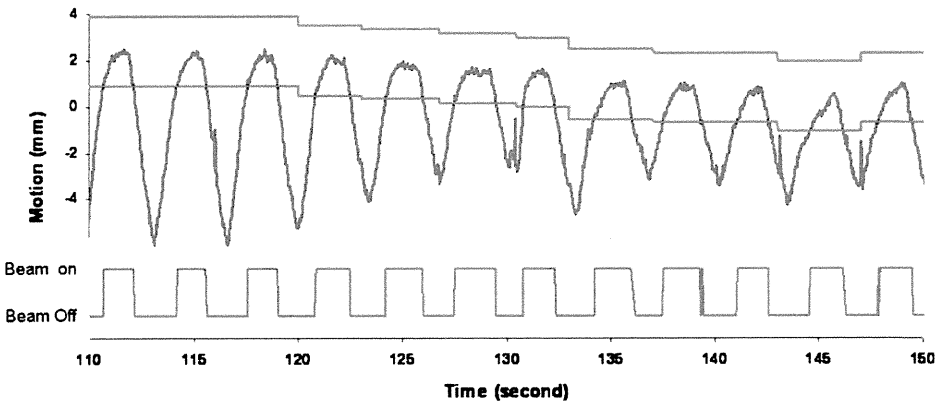

FIG. 6. This figure shows an amplitude-based ideal dynamic gating window being adjusted over the course of treatment.

model is highly variable. The gating window position of the dynamic gating approach is inconsistent for this type motion and the duty cycle is greatly affected.

Other than the duty cycle, several qualitative benefits were observed in the use of dynamic gating. In many of the fractions for which no duty cycle improvement was obtained, the EOE peak exited the static gating window, whereas with a dynamic window, the EOE peak was contained in the window. Two issues are masked by this apparent improvement in duty cycle. First, with the EOE peak exiting the gating window, a treatment interruption would be called for. However, this would likely be less than 2 s in duration, which is not achievable on most treatment machines. For the patient shown in Fig. 7, the instances of beam toggling are doubled for a fixed static window compared to the ideal dynamic window.

Another advantage of dynamic gating is shown in Fig. 8. The fixed gating window will require beam toggling nine times within three breathing cycles. Some of the beam toggles occur within 100 ms. The corresponding ideal dynamic window will only require three instances of beam toggling. For these three breathing cycles, the gating duty cycle changes from 34.4% to 47.7%.

Due to the noise in the motion signal and irregular breathing patterns, even with the ideal dynamic gating window, the amount of beam toggling is still substantial. A smoothing algorithm can be applied to avoid beam toggling caused by the noise signal. However, the beam toggling caused by irregular breathing patterns will not be solved by any smoothing algorithm. Additionally, it may be efficacious to recognize the location of the current EOE phase as it begins, rather than attempt to predict it *a priori*. The online FSM is able to do this with very short latency and modification of the online FSM for dynamic gating is another research direction for the presented work. At present, this is not feasible due to FSM

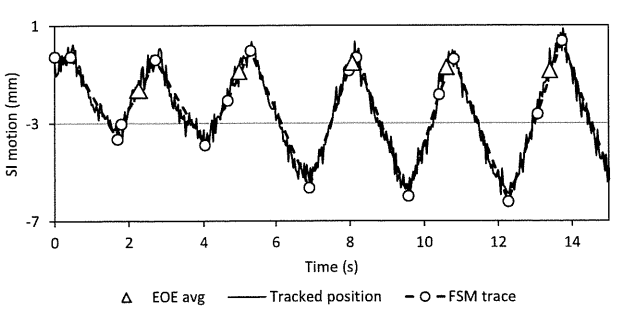

FIG. 7. Example of breathing pattern with poorly differentiated FSM transitions.

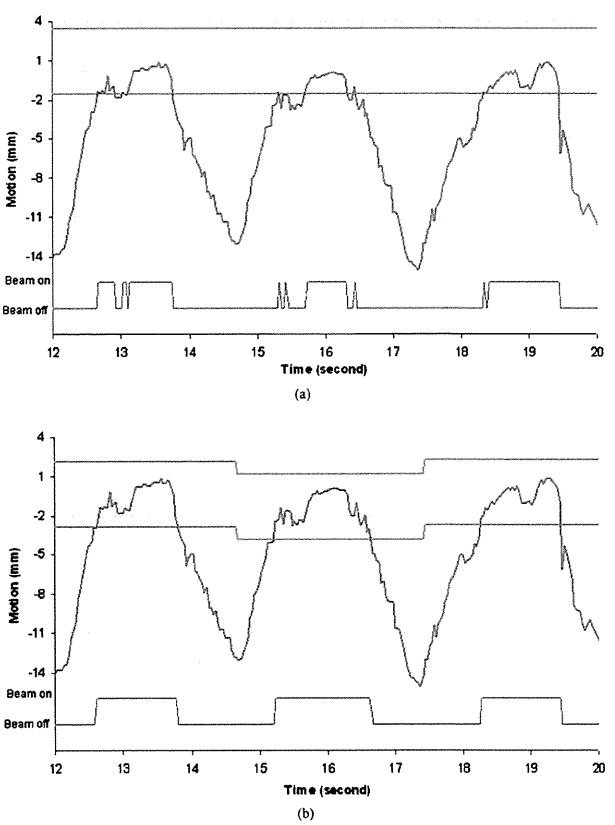

FIG. 8. Comparison of static and dynamic window showing scenario in which (a) static gating window requires additional rapid beam toggling and (b) the dynamic gating window perform better with less beam toggling and increased duty cycle. The gating window size is 5 mm in these two figures.

and mechanical system latencies, meaning that by the time the EOE phase is recognized and adjustments are made, it may already be over. A compromise could be informing the predicted location with a temporally closer phase, such as the immediately prior inhalation or exhalation phase.

Moreover, an interruption of the gating signal in the EOE phase is opposite the goals of EOE-based gating. The stability of the EOE phase is the reason for choosing it as the gating window and while a larger gating window that includes parts of the inhalation and exhalation phases might give a higher duty cycle, as sometimes occurs in the case of Fig. 7, the tumor would be in continuous motion while occupying that gating window. This trade-off of increased duty cycle for an unstable target would be clinically unacceptable. This suggests that further research is needed in placing the gating window in relation to the EOE phase and breathing phase transition points in order to minimize tumor motion within the gating window.

An additional factor that must be considered with the implementation of real-time treatment adjustments is how to redirect the radiation beam. In order to change the location of the gating window, either the patient must be moved through a treatment couch adjustment, or the radiation beam must be adjusted, possibly using a dynamic multileaf collimator. A side effect of such adjustments could be that while dose to the tumor is maintained, an increase in dose to surrounding normal tissue is introduced. Patient-specific limitations and boundaries would need to be determined *a priori* to ensure that the dose to critical structures is acceptable and quantifiable. Potential dose to normal tissue could possibly be quantified by overlaying the treatment plan on 4DCT images showing an anticipated adjusted anatomical state, i.e., temporally near the intended treatment phase. Such research and development is beyond the scope of this article, which will be investigated more in our ongoing research.

V. CONCLUSION

This paper proposed a dynamic gating approach to address the baseline shift problem caused by patient respiratory motion. Two methods of determining a dynamic gating window positions have been presented and analyzed. While dynamic gating did not guarantee an increased duty cycle for every patient, certain tumor locations and breathing motion patterns can see an increased duty cycle when dynamic gating is used. With duty cycle being just one factor in evaluating the efficacy of gated treatment, future research into the dosimetric implications of dynamic gating help determine if it is an attractive option for increasing the efficiency of respiratory-gated radiation therapy. Other qualitative considerations such as decreased beam toggling and increase tumor positional stability enhance the attractiveness of dynamic gating methods and require more research to quantify.

[a]Electronic mail: epepin@purdue.edu

[1]R. Li, J. H. Lewis, L. Cerviño, and S. B. Jiang, "A feasibility study of markerless fluoroscopic gating for lung cancer radiotherapy using 4DCT templates," Phys. Med. Biol. **54**, N489–N500 (2009).

[2]L. E. Butler *et al.*, "Dosimetric benefits of respiratory gating: A preliminary study," J. Appl. Clin. Med. Phys. **5**, 16–24 (2004).

[3]S. I. Denissova, M. H. Yewondwossen, J. W. Andrew, M. E. Hale, C. H. Murphy, and S. R. Purcell, "A gated deep inspiration breath-hold radiation therapy technique using a linear position transducer," J. Appl. Clin. Med. Phys. **6**, 61–70 (2005).

[4]M. Guckenberger *et al.*, "Potential of image-guidance, gating and real-time tracking to improve accuracy in pulmonary stereotactive body radiotherapy," Radiother. Oncol. **91**, 288–295 (2009).

[5]S. S. Korreman, T. Juhler-Nøttrup, and A. Boyer, "Respiratory gated-beam delivery cannot facilitate margin reduction, unless combined with respiratory correlated image guidance," Radiother. Oncol. **86**, 61–68 (2008).

[6]N. Linthout *et al.*, "Treatment delivery of time optimization of respiratory gated radiation therapy by application of audio-visual feedback," Radiother. Oncol. **91**, 330–335 (2009).

[7]E. Yorke, K. E. Rosenzweig, R. Wagman, and G. S. Mageras, "Interfractional anatomic variation in patients treated with respiration-gates radiotherapy," J. Appl. Clin. Med. Phys. **6**, 19–32 (2005).

[8]E. C. Ford, G. S. Mageras, E. Yorke, K. E. Rosenzweig, R. Wagman, and C. C. Ling, "Evaluation of respiratory movement during gated radiotherapy using film and electronic portal imaging," Int. J. Radiat. Oncol., Biol., Phys. **52**, 522–531 (2002).

[9]R. Muirhead, C. Featherstone, A. Diffton, K. Moore, and S. McNee, "The potential clinical benefit of respiratory gated radiotherapy (RGRT) in non-small cell lung cancer (NSCLC)," Radiother. Oncol. **95**, 172–177 (2010).

[10]A. Tai, J. D. Christensen, E. Gore, A. Khamene, T. Boettiger, and X. A. Li, "Gated treatment delivery verification with on-line megavoltage fluoroscopy," Int. J. Radiat. Oncol., Biol., Phys. **76**, 1592–1598 (2010).

[11]C. Nelson *et al.*, "Evaluation of tumor position and PTV margins using image guidance and respiratory gating," Int. J. Radiat. Oncol., Biol., Phys. **76**, 1578–1585 (2010).

[12]K. Ohara *et al.*, "Irradiation synchronized with respiration gate," Int. J. Radiat. Oncol., Biol., Phys. **17**, 853–857 (1989).

[13]C. G. Willett *et al.*, "The effect of the respiratory cycle on mediastinal and lung dimensions in Hodgkin's disease," Cancer **60**, 1232–1237 (1987).

[14]S. S. Korreman, A. N. Pedersen, T. J. Nøttrup, L. Specht, and H. Nyström, "Breathing adapted radiotherapy for breast cancer: Comparison of free breathing gating with the breath-hold technique," Radiother. Oncol. **76**, 311–318 (2005).

[15]H. H. Liu *et al.*, "Evaluation of internal lung motion for respiratory-gated radiotherapy using MRI: Part II—Margin reduction of internal target volume," Int. J. Radiat. Oncol., Biol., Phys. **60**, 1473–1483 (2004).

[16]S. Minohara, T. Kanai, M. Endo, K. Noda, and M. Kanazawa, "Respiratory gated irradiation system for heavy-ion radiotherapy," Int. J. Radiat. Oncol., Biol., Phys. **47**, 1097–103 (2000).

[17]R. W. M. Underberg, J. R. can Sörnsen de Koste, F. J. Lagerwaard, A. Vincent, B. J. Slotman, and S. Senan, "A dosimetric analysis of respiration-gated radiotherapy in patients with stage III lung cancer," Radiat. Oncol. **1**, 8–8 (2006).

[18]L. Dietrich, T. Tücking, S. Nill, and U. Oelfke, "Compensation for respiratory motion by gated radiotherapy: An experimental study," Phys. Med. Biol. **50**, 2405–2414 (2005).

[19]R. I. Berbeco, S. Nishioka, H. Shirato, and S. B. Jiang, "Residual motion of lung tumors in end-of-exhale respiratory gated radiotherapy based on external surrogates," Med. Phys. **33**, 4149–4156 (2006).

[20]Y. Cui, J. G. Dy, B. Alexander, and S. Jiang, "Fluoroscopic gating without implanted fiducial markers for lung cancer radiotherapy based on support vector machines," Phys. Med. Biol. **53**, N315–N327 (2008).

[21]S. S. Korreman *et al.*, "The role of image guidance in respiratory gated radiotherapy," Acta Oncol. **47**, 1390–1396 (2008).

[22]J. Cai *et al.*, "Effects of breathing variation on gating window internal target volume respiratory gated radiation therapy," Med. Phys. **37**, 3927–3934 (2010).

[23]R. E. Wurm *et al.*, "Image guided respiratory gated hypofractionated stereotactic body radiation therapy (H-SBRT) for liver tumors: Initial experience," Acta Oncol. **45**, 881–889 (2006).

[24]N. Koch *et al.*, "Evaluation of internal lung motion for respiratory-gated radiotherapy using MRI: Part I—Correlating internal lung motion with skin fiducial motion," Int. J. Radiat. Oncol., Biol., Phys. **60**, 1459–1472 (2004).

[25]N. M. Wink, M. Chao, J. Anthony, and L. Xing, "Individualized gating windows based on four-dimensional CT information for respiration-gated radiotherapy," Phys. Med. Biol. **53**, 165–175 (2008).

[26]W. C. Wu, C. L. Chan, Y. W. Wong, and J. P. Cuijpers, "A study on the